Fluctuations of coupled fluid and solid membranes with application to red blood cells

Thorsten Auth and S. A. Safran
Weizmann Institute of Science, Department of Materials and Interfaces, P.O. Box 26, Rehovot 76100, Israel

Nir S. Gov
Weizmann Institute of Science, Department of Chemical Physics, P.O. Box 26, Rehovot 76100, Israel
(Received 3 April 2007; revised manuscript received 1 August 2007; published 12 November 2007)

The fluctuation spectra and the intermembrane interaction of two membranes at a fixed average distance are investigated. Each membrane can either be a fluid or a solid membrane, and in isolation, its fluctuations are described by a bare or a wave-vector-dependent bending modulus, respectively. The membranes interact via their excluded-volume interaction; the average distance is maintained by an external, homogeneous pressure. For strong coupling, the fluctuations can be described by a single, effective membrane that combines the elastic properties. For weak coupling, the fluctuations of the individual, noninteracting membranes are recovered. The case of a composite membrane consisting of one fluid and one solid membrane can serve as a microscopic model for the plasma membrane and cytoskeleton of the red blood cell. We find that, despite the complex microstructure of bilayers and cytoskeletons in a real cell, the fluctuations with wavelengths $\lambda \gtrsim 400$ nm are well described by the fluctuations of a single, polymerized membrane (provided that there are no inhomogeneities of the microstructure). The model is applied to the fluctuation data of discocytes ("normal" red blood cells), a stomatocyte, and an echinocyte. The elastic parameters of the membrane and an effective temperature that quantifies active, metabolically driven fluctuations are extracted from the experiments.

DOI: 10.1103/PhysRevE.76.051910 PACS number(s): 87.16.Dg, 87.68.+z, 87.17.−d, 83.60.−a

I. INTRODUCTION

In this paper, we present theoretical predictions for the fluctuation spectra and the repulsive pressure of two interacting membranes that are maintained at a fixed average distance. Each individual membrane can show either fluid or solid fluctuation behavior. In the first part of this article, we discuss the theoretical aspects of the coupled membrane model. In the second part, we apply our model to analyze experimental data for fluctuation spectra of the red blood cell (RBC) membrane.

The theoretical description of noninteracting fluid membranes, such as bilayers or amphiphilic monolayers, is well known [1] and is confirmed by experiment [2] and simulation [3]. Solid membranes, which have a fixed connectivity of molecules and thus a shear elasticity, have been extensively studied in the past, mainly in connection with the crumpling transition. The properties of an isolated solid membrane are, for example, discussed in Refs. [4–6]. We are interested in the flat phase of solid membranes, since in the coupled-membrane model, this phase is additionally stabilized by the excluded-volume interaction between the two membranes. The initial self-consistent analytical models for solid membranes have been refined by simulations and perturbative calculations; for an overview, see Ref. [6].

The interaction between fluid membranes at fixed average distance is investigated in Refs. [7,8]; one membrane confined by parallel walls is discussed in Ref. [9]. The interaction of two solid membranes that fluctuate at fixed average distance is investigated in Ref. [10]; one membrane in between two parallel walls is discussed in Refs. [11,12]. A fluid membrane that interacts with a rough or a chemically patterned substrate is discussed in Refs. [13–15]; the influence of the discrete coupling of a fluid membrane to a substrate is studied in Ref. [16].

We generalize these studies and compare the fluctuation properties and interactions of two membranes. We particularly emphasize the interaction of one solid and one fluid membrane. Our theory goes beyond the model of two membranes coupled by a harmonic potential, since we use a microscopic model that takes into account the excluded volume of two membranes at fixed distance. We then derive the effective harmonic interaction potential that depends on the interaction constant v_0 and the elastic moduli κ (bending) and/or μ (shear), as well as the average intermembrane distance d.

We model the membranes by two surfaces in the Monge parametrization with appropriate elastic moduli. The membranes interact by the universal and generic excluded-volume interaction; the spacing is maintained by an external, homogeneous pressure p_e [see Fig. 1(a)]. If strongly coupled, the surfaces fluctuate as if they were one effective membrane with combined elastic properties [see Fig. 1(b)]. In this regime, the fluctuation in the intermembrane distance is relatively small in order to minimize the excluded volume interactions that arise from fluctuations at smaller wavelengths [17]. For weak coupling, both membranes only interact over small contact areas [see Fig. 1(c)]. Weak or strong coupling can be defined for specific ranges of fluctuation wave vectors. In the limit of very small wave vectors, the fluctuations are strongly coupled; for very large wave vectors, the fluctuations are weakly coupled.

The real-space Hamiltonian is treated in Fourier space where fluctuations with different wave vectors decouple. The propagators have a simple form, but the spectra show complex behavior. We predict that if one membrane is a solid membrane, three crossovers in the fluctuation spectrum as a function of the wave vector appear in the system. One crossover is due to the interaction of the bending and shear modes of the solid membrane: the effective bending rigidity is wave

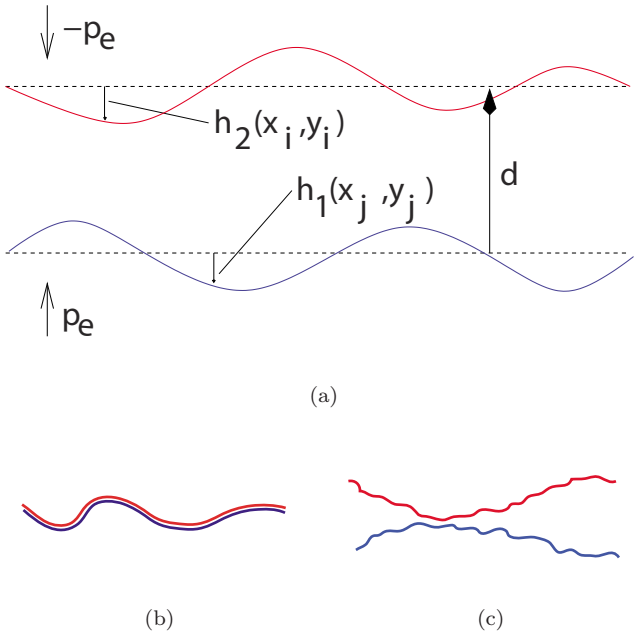

FIG. 1. (Color online) (a) Definition of the height fields $h_1(x,y)$ and $h_2(x,y)$. A homogeneous pressure p_e keeps both membranes at average mean distance d. The membranes interact if $h_1(x_i,y_i) = h_2(x_i,y_i)$. (b) If strongly coupled, both membranes fluctuate like a single membrane. (c) If weakly coupled—e.g., for fluctuation amplitudes that are small compared to the average intermembrane spacing—both membranes fluctuate independently. They only interact over relatively small areas, due to fluctuations on longer length scales.

vector independent at large wave vectors and renormalizes to larger values at small wave vectors. The second crossover is due to the transition between the coupled fluctuations of both membranes at small wave vectors and the mainly independent fluctuations at large wave vectors. Yet another crossover is found for the fluctuation pressure of a pair of one fluid and one solid membrane. If the solid membrane has a small constant bending modulus—like, for example, a polymerized membrane—the system acts like a solid membrane next to a wall at small spacings d. At large spacings, coherent long-wavelength fluctuations are possible and the bending modulus of the solid membrane is strongly renormalized. The system is well approximated by a fluid membrane next to a wall.

The architecture of a composite membrane that contains one fluid and one solid layer is used by cells to provide mechanical stability. One example are RBCs, which are constantly exposed to mechanical stresses in the blood flow. *In vivo*, RBCs live in the human vascular system for $\approx$120 days, despite constant exposure to flow and repeated strong deformations as they are squeezed through narrow capillaries [18,19]. Their lifetime is two orders of magnitude longer than that of artificial vesicles designed for use in drug delivery [20]. A network of flexible, spectrin polymers forms a two-dimensional cytoskeleton that completely covers the inner surface of the bilayer [21,22]. Within the approach presented in this article, the spectrin cytoskeleton is modeled as a solid membrane and the bilayer as a fluid membrane. RBCs are of obvious importance on their own; furthermore, the RBC membrane can serve as a model system for other mammalian cells [22–24]. Our model of a fluid and a solid membrane is one approach to take into account the microscopic features of the RBC membrane; we focus on the finite spacing between bilayer and cytoskeleton. Other recent approaches are discussed in Refs. [25–27]; in Ref. [28], a two-component network is studied by computer simulations that represents bilayer and cytoskeleton.

The shape transformations of RBCs as a function of the elastic moduli and the spontaneous curvature are well understood, although the microscopic origin of the spontaneous curvature is still unclear [29]. Much less is understood about the fluctuations of the cell membrane that have been measured in numerous studies that followed the seminal publication of Brochard and Lennon [30]. Apparently contradictory experimental results for the elastic properties and the fluctuations pose yet unresolved puzzles [31]. On the one hand, static deformation experiments show the cell membrane to be very stiff [32–35]. On the other hand, interferometric microscopy data suggest a very floppy membrane at fluctuation wavelengths of about 1 μm [36,37]. Furthermore, the fact that depletion or addition of adenosine triphosphate (ATP) changes the magnitude of the fluctuations indicates that thermal effects alone cannot explain the observations. ATP can be used to control the fluctuations in a physically interesting manner [38,39].

Bilayer-cytoskeleton interactions can be rather complex, depending on the architecture of the cytoskeleton and the chemical processes involved [40]. Electron micrographs suggest that the cytoskeletal spectrin network of RBCs assembles with a mesh size of 60–100 nm [41]. The average spacing between the spectrin and the bilayer is about $d = 30$ nm and is of the same order of magnitude as the root-mean-squared fluctuation amplitudes of the bilayer [36,42–44]. The analysis of the fluctuation spectrum allows us to characterize the elastic properties of the RBC membrane. The spectrum relates large-scale properties measured in static deformation experiments to the small length scales at which active effects of single ATP molecules are supposed to take place.

In the theoretical sections, we derive the coupled membrane model in Sec. II and we review the effective bending modulus of a solid membrane in Sec. III. In Sec. IV, we discuss the results of the coupled membrane model and compare them with simple scaling arguments. Details of the analytical calculations and further results can be found in the Appendixes.

In Sec. V, we apply our model to analyze the experimental RBC fluctuation spectra. In Sec. V A, we review the experimental papers and the theoretical models found in the literature. In Sec. V B, we analyze the fluctuation data of discocytes, an echinocyte, and a stomatocyte with the coupled membrane model and extract the elastic parameters. Using the phenomenological concept of an active temperature, we extract a measure for active, ATP-driven fluctuations in Sec. V C. In the Appendixes, we motivate the functional form of the effective bending modulus and show that the fluctuations of bilayer and cytoskeleton are strongly coupled for wavelengths $\lambda < 400$ nm.

II. CONTINUUM COUPLED MEMBRANES

We calculate the fluctuation spectra of two adjacent membranes that interact via their excluded volume. Height fields $h_1(x,y)$ and $h_2(x,y)$ describe the conformations of the membranes; see Fig. 1. The height variables are chosen relative to the average position of each membrane. The membrane fluctuations are governed by their curvature moduli κ_1 and κ_2. For fluid membranes, the curvature moduli are constants; solid membranes are represented by wave-vector-dependent, effective curvature moduli [4,5]. The functional forms of the bending moduli κ_i $(i=1,2)$ do not need to be further specified at this point and will be discussed later [45].

The real-space Hamiltonian for an almost flat system of two interacting membranes is

$$\mathcal{H} = \int d\boldsymbol{\rho} \left\{ \frac{1}{2}\kappa_1[\nabla^2 h_1(\boldsymbol{\rho})]^2 + \frac{1}{2}\kappa_2[\nabla^2 h_2(\boldsymbol{\rho})]^2 + v_0\delta(h_2(\boldsymbol{\rho}) - h_1(\boldsymbol{\rho}) - d) + p_e(h_2(\rho) - h_1(\rho)) \right\}, \quad (1)$$

where $\boldsymbol{\rho}=(x,y)$ is the coordinate pair in the plane. The only interaction between both membranes is the generic and universal excluded-volume interaction $v_0\delta(h_2(\boldsymbol{\rho})-h_1(\boldsymbol{\rho})-d)$. The interaction term is analogous to the classical treatment of self-avoiding polymers [47], and the interaction parameter v_0 has units of energy per length. The external pressure p_e acts as a Lagrange multiplier and constrains the constant average distance d between both membranes.

We use the δ-function interaction for mathematical convenience, and we estimate v_0 with an approximation similar to the Flory interaction for the excluded-volume interaction of polymers. If v_0 is large, the membranes are almost impenetrable and for two fluid membranes our results are very similar to those derived by Helfrich [8]. For the red blood cell, the volume of the spectrin molecules is smeared out over the entire area (200 nm filament contour length, 5 nm diameter, 2900 nm^2 area per filament); this yields an effective membrane thickness $d_s \approx 3$ nm. The thickness of the bilayer membrane is taken to be $d_b \approx$ 5nm. The probe volume is estimated by the spectrin diameter to be a cube with edge length $L_p=$ 5nm. After integrating out the in-plane components, the interaction constant reads $v_0=k_BT(d_s+d_b)/(2L_p^2) \approx 0.2k_BT\ \mathrm{nm}^{-1}$ [7].

The statistical mechanical properties of the real-space Hamiltonian are most easily treated with the help of a model Hamiltonian in Fourier space; all Fourier modes besides the zero-wave-vector mode $q=0$ serve as generalized coordinates [48]. The model Hamiltonian is taken to be a simple quadratic form in $|h_i(\mathbf{q})h_j(\mathbf{q})|^2$ $(i,j=1,2)$,

$$\mathcal{H}_0 = \left(\frac{2\pi}{L}\right)^2 k_BT \sum_{\mathbf{q}} \left[\frac{G_1(\mathbf{q})}{2} h_1(\mathbf{q})h_1(-\mathbf{q}) + \frac{G_2(\mathbf{q})}{2} h_2(\mathbf{q})h_2(-\mathbf{q}) + \frac{G_m(\mathbf{q})}{2}[h_1(\mathbf{q})h_2(-\mathbf{q}) + h_2(\mathbf{q})h_1(-\mathbf{q})] \right], \quad (2)$$

including all combinations $|h_1^2|$, $|h_2^2|$, and $|h_1h_2|$ [49]. The q-dependent coefficients $G_1(\mathbf{q})$, $G_2(\mathbf{q})$, and $G_m(\mathbf{q})$ are termed propagators in the remainder of the paper. The propagators G_1 and G_2 exactly account for the fluctuations of the noninteracting membranes, while the coefficient of the mixed term, G_m, accounts for the interaction.

The Bogoliubov inequality [7],

$$\mathcal{F} < \mathcal{F}_0 + \langle \mathcal{H} - \mathcal{H}_0 \rangle_0, \quad (3)$$

where $\mathcal{F}$ is the free energy of the system and $\langle \cdots \rangle_0$ is the average with respect to the model Hamiltonian, is employed and gives the upper bound for the exact free energy by minimizing with respect to G_1, G_2, and G_m. The Fourier transformations are defined by

$$h(\boldsymbol{\rho}) = \frac{1}{2\pi} \int d\mathbf{q} h(\mathbf{q}) \exp[-i\mathbf{q}\cdot\boldsymbol{\rho}] \quad (4)$$

for the height fields and

$$G(\boldsymbol{\rho}) = \frac{1}{(2\pi)^2} \int d\mathbf{q} G(\mathbf{q}) \exp[-i\mathbf{q}\cdot\boldsymbol{\rho}] \quad (5)$$

for the propagators. Instead of real-space coordinate pairs $\boldsymbol{\rho}$, now wave vectors $\mathbf{q}=(2\pi/\lambda_x, 2\pi/\lambda_y)$ and wavelengths λ_x and λ_y characterize the system. Transformation from continuous to discrete variables in Fourier space and vice versa is defined by

$$\left(\frac{2\pi}{L}\right)^2 \sum_{\mathbf{q}} = \int d\mathbf{q}, \quad (6)$$

where L is the system size, the sum runs from $(2\pi/L, 2\pi/L)$ to $(2\pi/a, 2\pi/a)$, and a is the lattice constant [7].

The total free energy to be minimized, $\tilde{\mathcal{F}}=\mathcal{F}_0+\langle \mathcal{H} - \mathcal{H}_0 \rangle_0$, is

$$\tilde{\mathcal{F}} = c_{\mathcal{F}} + \frac{k_BT}{2} \sum_{\mathbf{q}} \ln[G_1(\mathbf{q})G_2(\mathbf{q}) - G_m^2(\mathbf{q})] + \frac{1}{2}\sum_{\mathbf{q}} \kappa_1(\mathbf{q})\mathbf{q}^4 \frac{G_2(\mathbf{q})}{G_1(\mathbf{q})G_2(\mathbf{q}) - G_m^2(\mathbf{q})} + \frac{1}{2}\sum_{\mathbf{q}} \kappa_2(\mathbf{q})\mathbf{q}^4 \frac{G_1(\mathbf{q})}{G_1(\mathbf{q})G_2(\mathbf{q}) - G_m^2(\mathbf{q})} + v_0 L^2 \frac{e^{-d^2/(2\Delta^2)}}{\sqrt{2\pi}\Delta}, \quad (7)$$

with Δ the average root-mean-squared intermembrane distance,

$$4\pi^2\Delta^2 = \left(\frac{2\pi}{L}\right)^2 \left\langle \int d\boldsymbol{\rho} (h_1(\boldsymbol{\rho}) - h_2(\boldsymbol{\rho}))^2 \right\rangle, \quad (8)$$

and all constant terms are collected in $c_{\mathcal{F}}$. The statistical averages in phase space can only be calculated if $G_m^2(\mathbf{q}) < G_1(\mathbf{q})G_2(\mathbf{q})$, so that the quadratic form is positive definite. In the case $G_m^2(\mathbf{q}) > G_1(\mathbf{q})G_2(\mathbf{q})$, the statistical integrals would lead to divergent fluctuations and our Hamiltonian would be incorrect [46]. The solutions for the propagators have the form

$$G_i(\mathbf{q}) = \frac{\kappa_i(\mathbf{q})\mathbf{q}^4 + k_B T\chi^{-4}}{k_B T} \quad (i=1,2) \tag{9}$$

and

$$G_m = -\chi^{-4}, \tag{10}$$

with G_m completely independent of $\mathbf{q}$ and $G_1(\mathbf{q})$ and $G_2(\mathbf{q})$ a sum of a $\mathbf{q}$-dependent term and a constant excluded-volume potential $k_B T\chi^{-4}$. The constant term

$$k_B T\chi^{-4} = v_0(2\pi)^{9/2}\frac{(d^2-\Delta^2)}{(2\pi\Delta)^5}e^{-d^2/(2\Delta^2)} \tag{11}$$

is the same for all propagators. The excluded-volume potential $k_B T\chi^{-4}$ has dimensions of energy over length to the power of 4. The interaction length χ represents an effective distance between collisions. From the equations, we expect small intermembrane interactions in two cases: (i) for small relative mean-squared fluctuation amplitudes, $\Delta \ll d$, when the term $e^{-d^2/(2\Delta^2)}$ is small, and (ii) for large relative mean-squared fluctuation amplitudes, at $\Delta \approx d$, but only just before the model fails, such that the prefactor $(d^2-\Delta^2)/(\Delta^5)$ is small, but still non-negative. Note that the latter situation does not occur for real systems, since with increased crossing of the membranes, the repulsive interaction must increase.

Despite the simplicity of the propagators, the fluctuation spectra show complex behavior. The calculation of the fluctuation amplitudes involves combinations of propagators, so that, in general, both (effective) bending rigidities determine the fluctuations of each membrane. The mean values of the fluctuation amplitudes are

$$\langle|h_1(\mathbf{q})|^2\rangle = \left(\frac{L}{2\pi}\right)^2 \frac{G_2(\mathbf{q})}{G_1(\mathbf{q})G_2(\mathbf{q}) - G_m^2(\mathbf{q})}, \tag{12}$$

for the membrane described by h_1, while an analogous expression with exchanged indices, $1 \leftrightarrow 2$, holds for the membrane described by h_2. The mean-squared fluctuation of the intermembrane distance is

$$\langle|h_2(\mathbf{q}) - h_1(\mathbf{q})|^2\rangle = \left(\frac{L}{2\pi}\right)^2 \frac{G_1(\mathbf{q}) + G_2(\mathbf{q}) + 2G_m(\mathbf{q})}{G_1(\mathbf{q})G_2(\mathbf{q}) - G_m^2(\mathbf{q})}. \tag{13}$$

For small mean-squared fluctuation amplitudes compared with the squared intermembrane spacing d^2, the parameter χ becomes comparable to d; this occurs for high bending rigidities κ_i, or small interaction parameter v_0. In the lowest-order terms in a series expansion of Eqs. (12) and (13), for small values of χ^{-4}, the fluctuations of both membranes decouple (i.e., when $v_0=0$, for large values of κ_i or $d \to \infty$). We then recover the mean-squared fluctuation amplitudes of the isolated membranes,

$$\langle|h_i(\mathbf{q})|^2\rangle = \left(\frac{L}{2\pi}\right)^2 \frac{k_B T}{\kappa_i(\mathbf{q})\mathbf{q}^4} \quad (i=1,2). \tag{14}$$

In that case, the mean-squared amplitudes of the intermembrane distance are

$$\langle|h_2(\mathbf{q}) - h_1(\mathbf{q})|^2\rangle = \left(\frac{L}{2\pi}\right)^2 \left(\frac{k_B T}{\kappa_1(\mathbf{q})\mathbf{q}^4} + \frac{k_B T}{\kappa_2(\mathbf{q})\mathbf{q}^4}\right). \tag{15}$$

In the strong-coupling limit $\chi \to 0$ (appropriate for small values of κ_1, κ_2, or d), both membranes fluctuate as if they were a single composite membrane. The mean-squared fluctuation amplitudes

$$\langle|h_1(\mathbf{q})|^2\rangle = \langle|h_2(\mathbf{q})|^2\rangle = \left(\frac{L}{2\pi}\right)^2 \frac{k_B T}{\kappa_1(\mathbf{q})\mathbf{q}^4 + \kappa_2(\mathbf{q})\mathbf{q}^4} \tag{16}$$

are identical for both membranes. In this case, the mean-squared amplitudes of the intermembrane distance vanish,

$$\langle|h_2(\mathbf{q}) - h_1(\mathbf{q})|^2\rangle = 0. \tag{17}$$

The expansions of the fluctuation amplitudes of two membranes for small and for large χ, as well as further details of the calculations in this section, can be found in Appendix A.

III. EFFECTIVE BENDING RIGIDITY OF A SINGLE SOLID MEMBRANE

In this section, we review the fluctuation properties of an isolated solid membrane and summarize the results found in the literature.

For large wave vectors, a solid membrane has a wave-vector-independent bending modulus. This constant bending modulus can be estimated from the energy of a bent, thin elastic plate [51]. Its value

$$\kappa_c = \frac{b^2\mu}{6}\frac{1+\nu}{1+\nu^2} \tag{18}$$

depends on the two-dimensional shear modulus μ, the thickness of the solid membrane, b, and the Poisson ratio ν. Reasonable values for the Poisson ratio are $\nu=-1/3$, for a solid membrane represented by a free polymer network (which expands laterally if it is stretched) [6], or $\nu=1/2$, if a polymer network is coupled to a fluid membrane that preserves the area [51].

For networks of flexible polymers, typical bond stretching energies are of the order of $k_B T$ and typical bond lengths ℓ are in the range of a hundred nanometers to micrometers. The thickness of the spectrin cytoskeleton of red blood cells is estimated by the radius of gyration of the spectrin tetrameres, $b=R_g \approx 10-25$ nm. Because $\mu \approx k_B T/\ell^2$, this leads to a constant bending modulus of the network that is small compared with the typical bending moduli of lipid bilayer membranes [52]. Using a typical two-dimensional shear modulus of the RBC spectrin network (see Secs. V B and V C), $\mu = 10^{-2} k_B T\ \mathrm{nm}^{-2}$, we obtain $\kappa_c = (0.1-0.6)k_B T$. The wave-vector-independent part of the bending modulus can also be estimated with an excluded-volume approach in a model of beads connected by tethers. The excluded-volume approach provides an upper bound to the wave-vector-independent bending modulus, $\kappa_c \approx 1.1 k_B T$ [4].

For small wave vectors, the bending constant is considerably renormalized to higher values by the interaction between bending and shear modes [4,5]. The effective bending rigidity is given by [53,54]

$$\alpha_r \mathbf{q}^{-1} = \sqrt{\frac{3\mu k_B T}{4\pi}} \frac{1}{\mathbf{q}}; \tag{19}$$

see Appendix B [55]. Comparing the asymptotically constant bending rigidity κ_c for large q and the renormalized bending rigidity for small q given by Eq. (19), a crossover wave vector $q^* = \sqrt{3\mu k_B T/(4\pi)}/\kappa_c$ can be determined. For $q \ll q^*$, the bending rigidity is strongly renormalized as in Eq. (19); for $q \gg q^*$, the bending rigidity is constant as in Eq. (18).

For intermediate wave vectors, a perturbative treatment of the interaction between bending and shear modes may be appropriate. Instead of the summation of the entire set of diagrams from the perturbation expansion, which leads to the q^{-1} term, only the first two terms of the expansion need to be considered. The effective, renormalized bending rigidity is then given by [53,54]

$$\kappa_c + \alpha_p \mathbf{q}^{-2} = \kappa_c + \frac{9\mu k_B T}{16\pi\kappa_c} \frac{1}{\mathbf{q}^2}. \tag{20}$$

For details of the derivation, see Appendix B.

In addition to the constant bending rigidity and the renormalization due to the interaction of bending and shear modes, the presence of a nonzero average curvature of a solid membrane acts as a confining potential [51,56]. The strength of this potential,

$$\gamma = \frac{4\mu}{A} \int_A dS(2H^2 - K), \tag{21}$$

depends on the local mean curvature H and the local Gaussian curvature K, and is determined by an average over the membrane area A. Locally different values for the confinement potential can be obtained if A is not chosen to be the entire area of the system, but rather a smaller area around each point of the membrane. The confinement potential can be derived from the in-plane stretching energies that occur if the radius of a sphere or a cylinder is changed; for details, see Appendix B.

For the theoretically motivated calculations in Sec. IV, we only use the self-consistent result of Eq. (19) for all calculations that involve the effective bending rigidity of the solid membrane. We restate this in the next section, which starts with a more general discussion in the introduction. The perturbative treatment of the shear-bending interaction and the confinement potential, given in Eqs. (20) and (21), will be used for the analysis of the red blood cell fluctuation data in Secs. V B and V C. We show in Appendix E that the perturbation form of Eq. (20) is more appropriate than the self-consistently calculated Eq. (19) when considering the experimental data.

IV. RESULTS OF THE COUPLED MEMBRANE MODEL: FLUCTUATION PRESSURE

In this section, we first discuss limiting cases for a fluid-solid system: coupled and uncoupled fluctuations of both membranes, shear-bending renormalized, and wave-vector-independent bending moduli of the solid membrane. In the rest of the section, we assume the bending constant of the solid membrane to be strongly renormalized as described by Eq. (19). Thus the solid membrane considered in this section is always assumed to be flat on average, such that $\gamma=0$ [Eq. (21)]. The fluctuations of the fluid membrane are governed by a wave-vector-independent bending modulus κ_f.

If a solid membrane fluctuates next to a fluid membrane, there are four possible combinations of limiting cases for the fluctuation behavior for small and large q. In the case of weak interactions between both membranes and for wave vectors $q > q^*$ [q^* defined after Eq. (19)], Eqs. (14) and (18) apply. The fluctuations of each membrane are determined by its individual, wave-vector-independent, bending modulus. This case is analogous to the fluctuations of two fluid membranes. For weak interactions between the membranes and for $q < q^*$, Eqs. (14) and (19) apply. The fluctuations of the fluid membrane are described by its wave-vector-independent bending modulus, while the fluctuations of the solid membrane are governed by its renormalized bending modulus at small wave vectors, $\alpha_r q^{-1}$. In the strongly coupled regime of Eq. (16), both membranes fluctuate together with negligible fluctuations of their intermembrane distance, Eq. (17). These strongly coupled fluctuations are governed by the sum of the bending rigidities of the fluid and the solid membrane. Instead of κ_c, now $\kappa_f + \kappa_c$ must be used to calculate the new crossover wave vector for the bending-shear interaction, q^*. For $q > q^*$, the combined bending rigidity is a constant. For $q < q^*$, the bending rigidity is renormalized due to the shear-bending interaction.

In Appendix C, simple scaling arguments for the mutual confinement of the fluctuations of both membranes, valid in the limit $v_0 \to \infty$, are presented. We also introduce a crossover wave vector q^+, below which the fluctuations of the two membranes are coupled and above which the fluctuations are uncoupled [17]. The free energy per membrane area, needed to evaluate the fluctuation pressure, is discussed in Appendix D. Here, we calculate the repulsive fluctuation pressure with the coupled membrane model for different system parameters. We apply simple scaling arguments to discuss the origin of the crossover in the fluctuation behavior for a fluid-solid system. The crossover is correlated to the fraction of the intermembrane spacing occupied by the fluctuations of the fluid, d_f/d, and by the solid membrane, d_s/d.

Fluctuation pressure. The repulsive pressure between both membranes, $p = -\partial \mathcal{F}/\partial d$, can be calculated from the free energy. With simple scaling arguments, the fluctuation pressure of a membrane is obtained from the negative derivative of the free energy difference, given for two fluid and two solid membranes in Eqs. (D1) and (D2), with respect to the confinement d. The fluctuation pressure of a fluid membrane with root-mean-squared fluctuation d_f is

$$p_f \sim \frac{(k_B T)^2}{\kappa_f d_f^3}. \tag{22}$$

The fluctuation pressure of a solid membrane with root-mean-squared fluctuation d_s is

$$p_s \sim \frac{(k_B T)^2}{\mu d_s^5}. \tag{23}$$

For a fluid-solid membrane pair, one can determine whether the fluctuations of the fluid or of the solid membrane at a

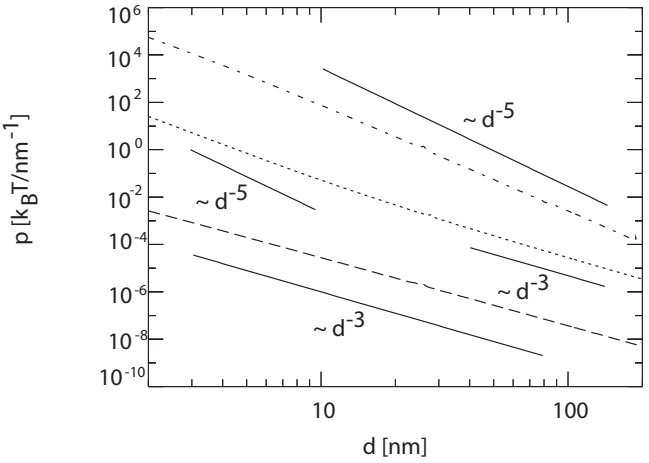

FIG. 2. Repulsive pressure p between both membranes as a function d for different systems: two fluid membranes (dashed line), two solid membranes (dash-dotted line), and one solid and one fluid membrane (dotted line). Same parameters as in Fig. 7. The numerical result for the solid membranes has been multiplied by 10^4, the result for the fluid-solid membrane by 10^2. For the fluid-solid system, a crossover between solidlike and fluidlike scaling is observed.

specific d dominate the scaling behavior by comparing their fluctuation pressures. The fluctuations of the membrane with the largest fluctuation pressure at the midplane, $d/2$, dominate.

For small enough d, the fluctuation pressure of the solid membrane always exceeds the fluctuation pressure of the fluid membrane, due to the d^{-5} scaling compared to the d^{-3} scaling. For large d, the pressure of the fluid membrane decays slower than the pressure of the solid membrane; thus, the fluctuation pressure of the fluid membrane dominates. The crossover d^* occurs for $p_f(d^*/2)=p_s(d^*/2)$. Numerical results for the fluctuation pressure are shown in Fig. 2, for the same systems used for χ in Fig. 7. The fit to the result of the fluid membranes scales like $d^{-2.9}$, close to the d^{-3} scaling found in Refs. [7–9]. The fit to the result of the solid membranes gives a scaling exponent −4.5, close to the d^{-5} scaling derived in Ref. [10]. Again, the values in the literature are obtained with our model in the limit $v_0 \to \infty$, because in this limit there is no other length scale in the model besides d. For the pair of one fluid and one solid membrane, we find a crossover between solidlike scaling at small d and fluidlike scaling at large d, similar to the behavior observed for χ in Fig. 7.

Simple scaling arguments explain the crossovers between fluidlike and solidlike scaling of the fluid-solid system. A virtual wall separates the membranes, and the fraction of the average spacing occupied by the fluctuations of each membrane, d_x/d, can be calculated from the d that minimizes the sum of the free energies, $\Delta f_f + \Delta f_s$ [Eqs. (D1) and (D2)].

For two identical membranes, both membranes have the same "effective thicknesses"; see Fig. 3(b). For two membranes of the same type with different elastic constants, the two "effective thicknesses" are not equal, but their ratio does not depend on d. For one solid and one fluid membrane, the behavior is more complex, as evident by the crossovers found for the fluctuation pressure, the interaction length, and

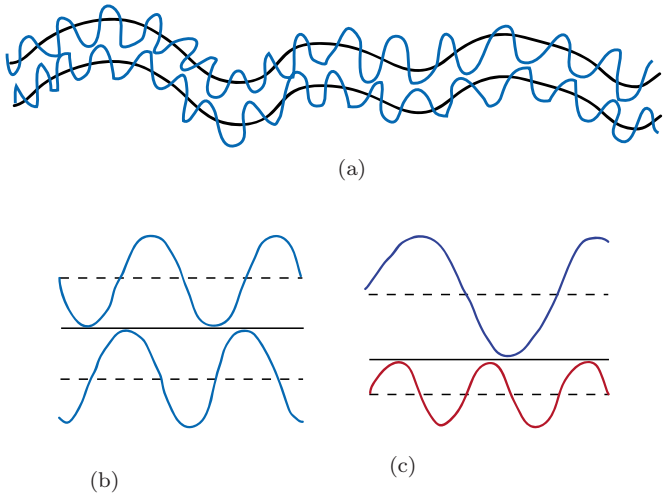

FIG. 3. (Color online) (a) Coupling of fluctuations at small wave vectors due to fluctuations at large wave vectors. (b) For two identical membranes, both membranes have the same effective thicknesses. (c) For two different membranes, generally the effective thicknesses of both membranes are not the same. For a pair of one solid and one fluid membrane, at small d the effective thickness the solid membrane is greater than the effective thickness of the fluid membrane; vice versa at large d.

the free energy differences and in Figs. 2, 7, and 9, respectively. The ratios between the effective thicknesses of both membranes vary with d. For small d and a small renormalization of the bending modulus of the solid membrane, the solid membrane occupies the larger fraction of the volume between both membranes and dominates the scaling. For large d, where long-wavelength fluctuations are allowed and the bending modulus of the solid membrane is considerably renormalized, the fluctuations of the fluid membrane dominate.

The fractions d_x/d are plotted in Fig. 4 for the same parameters as used in Figs. 2 and 7. As discussed earlier, for large enough d the solid membrane acts as a wall; see also Ref. [25] where this approximation is used to describe the red blood cell bilayer and the spectrin cytoskeleton. The crossover of the effective thicknesses of both membranes occurs roughly at the value of d where also the crossover in Figs. 2 and 7 has been observed.

V. RBC FLUCTUATIONS

We apply the coupled membrane model to analyze the experimental RBC fluctuation data of Refs. [36,37]. We first review other theoretical approaches found in the literature and investigate the applicability of the coupled-membrane approach. We then analyze the fluctuation data, extract the bilayer bending modulus κ_b and the spectrin shear modulus μ, and introduce a phenomenologically motivated effective temperature to account for actively driven fluctuations.

A. Experimental data and theoretical models

In this subsection, we review the current status of the theory for the RBC membrane fluctuations and highlight the gaps that exist in our present knowledge.

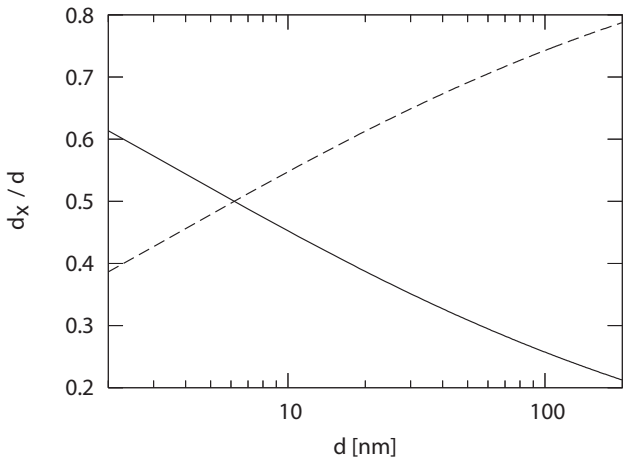

FIG. 4. Fraction of the spacing occupied by the effective thickness of the solid membrane, d_s/d (solid line), and the fluid membrane, d_f/d (dashed line), in a pair of one solid and one fluid membrane as function of the intermembrane spacing d. The same elastic parameters as in Fig. 7 have been used, but with the model sketched in Fig. 3(c) instead of the full self-consistent coupled membrane calculation.

In Refs. [36,37], specialized experimental and evaluation techniques were used to measure the fluctuation spectra of RBCs. The fluctuation data indicate that the effective bending modulus for fluctuations at small wave vectors is larger than the bending modulus for fluctuations at large wave vectors; see Figs. 5 and 6. This is consistent with the theoretical expectations for a system with a nonzero shear modulus and of finite area [57]. In Secs. V B and V C, we analyze the experimental data using our coupled membrane model [58,59].

In Ref. [25], the fluctuation data of Ref. [36] was plotted as a function of the wave vector after normalization by the fluctuations of a free, fluid bilayer. This emphasizes the data

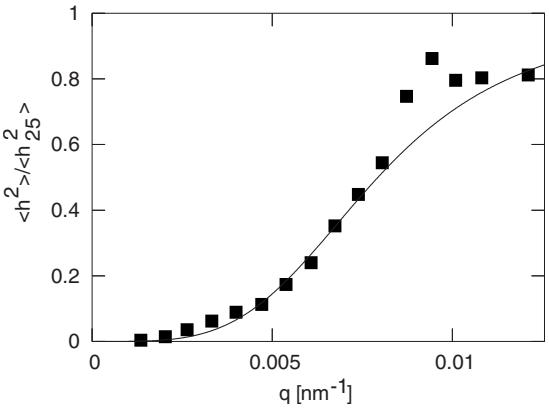

FIG. 5. Experimental fluctuation data for an echinocyte (Ref. [36]) and fit with a strongly coupled bilayer and polymerized membrane, represented by a single, effective membrane with bending modulus $\kappa_s(q)=\kappa_b+\alpha_p q^{-2}+\gamma q^{-4}$. The fluctuation amplitudes are normalized by the fluctuation amplitudes of a free membrane with $\kappa=25k_BT$, $\langle h_{25}^2\rangle$. The values of the fit parameters are given in the text.

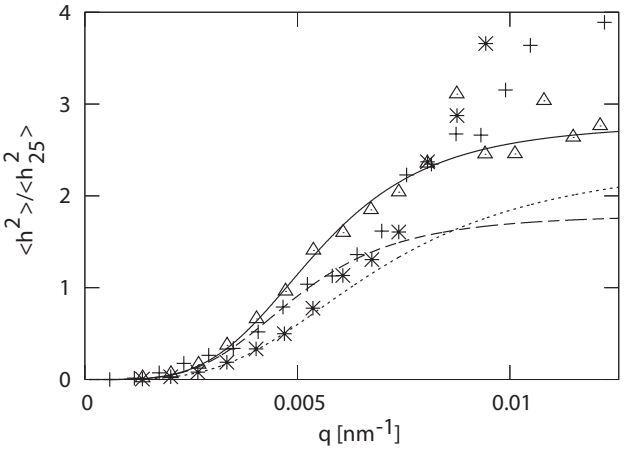

FIG. 6. Fit of the experimental data of Refs. [36,37] with a strongly coupled bilayer and polymerized membrane, represented by a single, effective membrane with bending modulus $\kappa_s(q)=\kappa_b+\alpha_p q^{-2}+\gamma q^{-4}$: discocyte 1 (+, dashed line, Ref. [37]), discocyte 2 (*, dotted line, Ref. [36]), stomatocyte (triangles, solid line, Ref. [36]). The fluctuation amplitudes are normalized by the fluctuation amplitudes of a free membrane with $\kappa=25k_BT$, $\langle h_{25}^2\rangle$. Values of the shear moduli and effective temperatures are given in the main text. Some of the experimental data points at high q for the discocytes are out of the plotted range because of their large fluctuation amplitudes.

at large wave vectors, and a jump in the spectrum becomes apparent. Above a threshold wave vector $q_0 \approx 0.008$ nm^{-1}, the fluctuation amplitudes show an unexpected increase. Reference [25] provided a good phenomenological description of the experimental data using an effective bending rigidity $\kappa_{\text{eff}}(q)=\kappa_b+\sigma q^{-2}+\gamma q^{-4}$. The wave-vector-independent bending modulus of the lipid bilayer, κ_b, surface tensions σ_1 for $q<q_0$ and $\sigma_2<\sigma_1$ for $q>q_0$, and a confining potential γ were used as fit parameters. It was shown that this description can be used to fit both the static as well as the dynamic data.

It was beyond the scope of Ref. [25] to discuss details of the physical origin of the fluctuation spectrum. The potential term was motivated by thinking of the cytoskeleton as a rigid wall that confines the fluctuations of the bilayer. A typical distance between bilayer and cytoskeleton was found ($d \approx 30$ nm) that matches experimental measurements of the thickness of the spectrin layer [42]. For large wave vectors, the fluctuation amplitudes are mainly determined by the constant, bare bending modulus of the lipid bilayer. An apparent jump in the surface tension was proposed to be the origin of the jump in the experimental data. For small wave vectors, a large surface tension was attributed to the periodic attachment of the bilayer to the skeleton. A tension term that originates from a periodic, sparse confinement of a bilayer was further discussed in Refs. [16,60]. For large wave vectors, the surface tension was found to have a small value that can be explained by the closed shape of the cell [57].

Two more detailed, recent theoretical models also reproduce the jump observed in the experimental data using different physical approaches. In Ref. [26], the bilayer experiences a surface tension due to its connections to a two-

dimensional network of sparsely attached springs that model the spectrin skeleton. In Ref. [61], this picture was further advanced and cytoskeletal defects were added to the model. By identifying the wave vector of the jump with the inverse mesh size of the cytoskeleton, the authors claim to explain the experimental data [26]. However, the usual relation between wave vector and wavelength is $q=2\pi/\lambda$ and not $q=1/\lambda$ as stated in Ref. [26]. Using $q=2\pi/\lambda$, the jump in the experimental data corresponds to wavelengths $\lambda>500$ nm, which are much larger than the mesh size of the spectrin network that forms the skeleton of the RBC ($\approx 60-100$ nm). The mismatch of the wave vector at which the increased fluctuation amplitudes are found in the experiment (≈ 0.008 nm^{-1}) and the wave vector that corresponds to the mesh size of the cytoskeleton anchors ($\approx 0.03-0.05$ nm^{-1}) raises questions on the relevance of the bilayer-spring model to interpret the data of Ref. [36].

In the theoretical model in Ref. [27], the bilayer is coupled to a three-dimensional, elastic gel. Using a three dimensional gel to model the spectrin layer is questionable, because the distance between cross-links in the cytoskeleton is 60–100 nm and thus of the same order as (or even larger than) its thickness ($2d\approx 60$ nm) [42,43]. The model does explain the jump in the experiment at large q, but is not able to explain the spectrum at small q. It is argued in Ref. [27] that the experimental data are not reliable at long wavelengths, since the boundary effects due to the closed shape of the cell are not properly taken into account by the Fourier transformation. However, the fit in Ref. [27] already begins to fail for wavelengths $\lambda\approx 1$ μm, which are small compared to the cell diameter $d_c=7-8$ μm. In addition, we expect the fluctuation Fourier amplitudes in a closed system to be smaller than the amplitudes of a free membrane with the same elastic constants. If the closed-shape argument were to apply, the fluctuation amplitudes predicted by the theory of Ref. [27] for a flat membrane would be larger than those found in experiment. The Fourier amplitudes predicted in Ref. [27] are considerably smaller than those measured in the experiment. Thus, the model of the three-dimensional elastic gel does not seem to be appropriate to describe the thin spectrin network of the RBC.

Our coupled membrane model focuses on the finite spacing between the lipid bilayer and the spectrin layer. At small wave vectors, bilayer and spectrin layer are strongly coupled [17]. At large wave vectors, bilayer and spectrin layer fluctuate independently. This decoupling could (qualitatively) lead to an increase of the fluctuation amplitudes of the bilayer (compared with the coupled bilayer and cytoskeleton fluctuations) that explains the jump observed in the experiments. The coupled membrane approach is applied to discocyte fluctuation data in Appendix E. We find that for wavelengths $\lambda>400$ nm—i.e., for the available experimental data—the fluctuations are well described by a *single* membrane with an effective bending rigidity of the form $\kappa_2(q)=\kappa_b+\alpha_p q^{-2}+\gamma q^{-4}$. Thus, similar to the other theoretical models, our coupled-membrane model does not reproduce the jump in the experimental spectra, but gives a good description of the data for $q\lesssim 0.008$ nm^{-1}.

However, in contrast to the models discussed before, our model is, in principle, free of fit parameters; all parameters can be measured independently in different experiments. In practice, not all the parameters needed to predict the fluctuation spectrum have been measured for those cells for which the spectrum has been measured (e.g., the shear modulus). For typical values of the parameters, the model is not sensitive to exact values of the spacing d and the interaction parameter v_0. The interaction parameter $v_0=0.2k_BT$ nm^{-1} is estimated using a Flory-type argument in Sec. II, and we use $d=30$ nm [42]. The model crucially depends on the values of the elastic constants κ_b and μ. These elastic constants vary for different cells and strongly depend on the experimental conditions [18,32–35,62–65]. We are thus forced to consider the bilayer bending rigidity and the spectrin shear modulus as fit parameters, within a plausible range of values. In the following subsections, we analyze the experimental RBC fluctuation data of Refs. [36,37].

B. Echinocyte, discocyte, stomatocyte

A single composite membrane with an effective bending modulus $\kappa_2(q)=\kappa_b+\alpha_p q^{-2}+\gamma q^{-4}$ is fit to the bilayer fluctuation data of several cells from Refs. [36,37].

In Fig. 5, we are able to fit the data for a RBC with the echinocyte shape from Ref. [36] in the entire q range, where κ_b, μ, and the value of the shape integral that enters γ [Eq. (21)] are independent fit parameters (since we do not know the exact shape of the echinocyte). We find $\kappa_b=25k_BT$, $\alpha_p=8.8\times 10^{-8}k_BT$ nm^{-2} and $\gamma=7.4\times 10^{-8}k_BT$ nm^{-4}. The shear modulus that corresponds to this value of α_p is $\mu=6\times 10^{-3}k_BT$ nm^{-2}. The confinement potential of the echinocyte, γ, is a factor of 5 larger than the corresponding term for the discocyte analyzed in Appendix E [66]. From Eq. (21), a larger value of γ is expected for the echinocyte due to the larger average curvature of the spicules that decorate the cell.

For the other cells, as shown in the fits in Fig. 6, we obtain $\kappa_b=14k_BT$ and $\mu=0.7\times 10^{-2}k_BT$ nm^{-2} for discocyte 1, $\kappa_b=10k_BT$ and $\mu=1.2\times 10^{-2}k_BT$ nm^{-2} for discocyte 2, and $\kappa_b=9k_BT$ and $\mu=0.3\times 10^{-2}k_BT$ nm^{-2} for the stomatocyte (if the data is associated with fluctuations of the concave side of the stomatocyte [67]). The shear moduli are obtained from the values of γ [68]. The confinement potential $\gamma\sim\mu$ is estimated to be $\gamma=1.2\times 10^{-6}\mu$ nm^{-2} for the discocyte, $\gamma=3.0\times 10^{-6}\mu$ nm^{-2} for the concave, and $\gamma=3.9\times 10^{-7}\mu$ nm^{-2} for the convex side of the stomatocyte, using the cell shapes provided in Ref. [69].

The shear moduli μ from the fits are in the range or slightly above the values found in many static deformation experiments, $\mu\approx 10^{-3}k_BT$ nm^{-2} [32–35]. All fit values are far below the value of $\mu\approx 5\times 10^{-2}k_BT$ nm^{-2}, measured in Ref. [65]. The various values for κ_b extracted from these fits are puzzling since we expect the lipid bilayer bending constant to be independent of the shape of the RBC. This puzzle is resolved by (phenomenologically) taking into account the different "effective temperatures" of the cells, T_{eff}, due to cell activity [38,39]. Since the data only provide us with the ratio κ_bT/T_{eff}, cells with different effective temperatures can have different *apparent* bending moduli when measured relative to k_BT. We show in the next section that the lipid con-

tribution to the bending moduli of all cells is the same, relative to the effective thermal energy $k_BT_{\rm eff}$.

C. Effective temperature

We introduce the effective temperature as a phenomenological concept to quantify active, nonthermal fluctuations [38,39,70–73]. We do not aim to identify the source of active processes in this article; cytoskeletal processes [39,74–76] as well as conformation changes of transmembrane proteins [70–72,77,78] have been suggested in the literature. In Refs. [38,39], active (ATP-driven) fluctuations for discocytes have been quantified by an effectively higher temperature $T_{\rm eff} \approx 2T-3T$. We thus reinterpret the *bare* bilayer bending constants to be a factor $T_{\rm eff}/T$ larger than the values obtained from the fits [79]. The larger values of the bare bilayer bending modulus ($\kappa_b \approx 25k_BT$) are indeed consistent with the values expected for such membranes from tether pulling [62], frequency spectra [63], simulations of cells in flow [18], and artificially produced phospholipid bilayers [64].

The fluctuation spectrum with an effective temperature $T_{\rm eff}$ is given by

$$\langle |h(q)|^2 \rangle = \frac{k_BT_{\rm eff}}{\kappa_2(q)q^4} = \frac{k_BT_{\rm eff}}{\kappa_b q^4 + \kappa_{p,\rm Teff} q^2 + \gamma} = \frac{k_BT}{f_T\kappa_b q^4 + \kappa_{p,T} q^2 + f_T\gamma}, \quad (24)$$

where $f_T=(T/T_{\rm eff})<1$ and $\kappa_{p,\rm Teff}$ refers to $\kappa_{p,\rm Teff}=9\mu k_BT_{\rm eff}/(16\pi\kappa_b)\sim k_BT_{\rm eff}$. Note that the effective temperature cancels in the q^2 term, $\kappa_{p,T}=9\mu k_BT/(16\pi\kappa_b)\sim k_BT$. After normalization, the fluctuation spectrum is

$$\frac{\langle |h(q)|^2 \rangle}{\langle |h_{25}(q)|^2 \rangle} = \frac{25k_BT}{(T/T_{\rm eff})\kappa_b + \alpha_p q^{-2} + (T/T_{\rm eff})\gamma q^{-4}}. \quad (25)$$

The echinocyte shape can be obtained experimentally by depletion of ATP, while the presence of ATP is known to increase the fluctuation amplitudes [38,39]. It thus seems reasonable to use the high-q plateau value of the fluctuation amplitudes of the echinocyte to estimate the bare bilayer bending modulus for *all* cells in the absence of active effects ($T_{\rm eff}=T$), $\kappa_b=25k_BT$. The smaller values obtained in the fits can then be used to quantify the active effects of the discocytes and the stomatocyte.

The effective temperatures and the shear moduli are $T_{\rm eff}/T=1.8$ and $\mu=1.3\times10^{-2}k_BT$ nm^{-2} for discocyte 1 in Fig. 2, $T_{\rm eff}/T=2.5$ and $\mu=3.0\times10^{-2}k_BT$nm^{-2} for discocyte 2 in Fig. 2, $T_{\rm eff}/T=2.8$ and $\mu=3.4\times10^{-2}k_BT$ nm^{-2} for the discocyte in Fig. 1, and $T_{\rm eff}/T=2.8$ and $\mu=0.8\times10^{-2}k_BT$ nm^{-2} for the stomatocyte in Fig. 2 (if the data are associated with fluctuations of the concave side [80]). With these values of $T_{\rm eff}$, all cells, independent of their shape, show the same bare bending rigidity $\kappa_b\approx25k_BT$ that is expected for a lipid bilayer.

The shear moduli obtained by our fits are large compared with the value found in many static deformation experiments, $\mu\approx10^{-3}k_BT$ nm^{-2} [32–35]. However, all values from the fit are still below the value of $\mu\approx5\times10^{-2}k_BT$ nm^{-2}, measured in Ref. [65]. The shear modulus of the stomatocyte is small compared to the shear moduli of the discocytes, due to its weak cytoskeleton [39]. The small shear modulus of the stomatocyte is consistent with strong active effects and a high effective temperature.

VI. CONCLUSIONS

A. Coupled-membrane model

We have presented a continuum model for pairs of membranes that fluctuate at a fixed average distance. Our model can be applied to membranes with arbitrary wave vector dependence of their effective bending moduli (this includes, for example, polymer-decorated membranes [81,82]), and arbitrary combinations of different membranes can be analyzed. The two membranes interact via the universal and generic excluded-volume interaction and the average distance is fixed by a homogeneous pressure. We applied our model to a pair of fluid membranes, to a pair of solid membranes, and to adjacent fluid and solid membranes.

For large interaction parameter v_0 and a fluid-fluid or a solid-solid system, our calculations agree with simple scaling relations for the interaction length χ, the characteristic wave vector $\tilde{q}$, and the repulsive fluctuation pressure p as a function of the average distance between the membranes, d. A crossover wave vector q^+ is introduced, below which the membranes fluctuate in a strongly coupled manner and above which the fluctuations are only marginally coupled. Strong coupling arises due to the excluded-volume interactions from fluctuations at smaller wavelengths [17].

Several forms of effective bending rigidities are relevant for the coupled-membrane system. For weak coupling, the membrane fluctuations are governed by their individual bending constants. In the strongly coupled limit, both membranes fluctuate like a single surface with an effective bending rigidity that is the sum of the individual bending rigidities. In addition, if a solid membrane is involved, for small q, the interaction between bending and shear modes renormalizes the bending modulus to higher values. The crossover wave vector below which the renormalization becomes important, q^*, depends on the values of the shear and the bare bending modulus; it thus has different values if the membrane fluctuations are strongly coupled (in which case the relatively large, lipid bending modulus must be included in the calculation of q^*) compared to the case in which the fluctuations are uncoupled (when for a polymer network only the small, solid bending modulus is used to find q^*).

For a pair consisting of one solid membrane and one fluid membrane, we also find a crossover with respect to the intermembrane distance d. For small d, all physical quantities related to the interaction show the scaling expected for a solid membrane next to a wall. For large d, the scaling of a fluid membrane next to a wall is found. The "effective thickness", or relative occupied intermembrane volume (Fig. 3), of both membranes can be calculated: for small d the fluctuations of the solid membrane occupy most of the intermembrane volume, while for large d the fluctuations of the fluid membrane almost fill the entire volume between both membranes.

We have also calculated the free energy difference per membrane area between the coupled and uncoupled membranes for a fluid-solid membrane pair. Numerical results are presented for different spacings d and for elastic parameters and an interaction parameter that are appropriate to biological systems such as red blood cells. The free energy difference is calculated as a function of the shear modulus, and the effect of the fluctuations of a solid membrane compared to a hard wall at the same average distance can be estimated. Strong fluctuations of the solid membrane considerably increase the free energy needed to keep the two membranes at an average distance d.

Simple scaling arguments explain the crossovers found for the interaction length and the fluctuation pressure with the coupled membrane model for a fluid-solid membrane pair. The solid membrane is assumed to be on average flat and to fluctuate at wave vectors well below the crossover q^*, where the shear-bending renormalization is significant. The membrane, the fluctuations of which fill the larger fraction of the volume in between both membranes, dominates the scaling relations. At small d, solidlike scaling is observed, while at large d, fluidlike scaling is found.

Our results about the scaling, intermembrane pressure, and fluctuation spectrum of two coupled membranes can be applied to various cellular membranes—e.g., to the red blood cell as well as to the nuclear envelope [83]. The results are also relevant for synthetic systems where a fluid and a polymerized membrane are coupled; this architecture might be used for drug-delivery schemes. Currently, more rigid actin networks are attached to artificial lipid bilayers for scaffolding purposes [84,85].

B. Red blood cell fluctuations

The coupled membrane model suggests that at wave vectors relevant to the experimental data in Refs. [36,37], $q < 0.015\text{nm}^{-1}$, both the cytoskeleton and the bilayer fluctuate in a strongly coupled manner. The physical origin of this effect is the excluded-volume interaction between the two layers due to fluctuations at shorter wavelengths [17]. Because of the complex architecture of the lipid bilayer and spectrin skeleton, this finding is not trivial. Using a microscopic model, we argue that the discrete, sparse coupling of and the finite spacing between lipid bilayer and spectrin cytoskeleton are only relevant for fluctuation wavelengths shorter than 400 nm.

For fluctuation wavelengths larger than 400 nm, our work justifies using a *single* effective membrane to model the red blood cell membrane. Its fluctuations are governed by the lipid bilayer bending rigidity and a two-dimensional shear modulus that arises from the spectrin network in this range of wave vectors. The coupled bending-shear fluctuations give rise to a surface-tension-like contribution as well as a confinement potential term that must be added to the lipid bilayer bending rigidity. This is consistent with the phenomenological treatment of Ref. [25].

The continuum model can reproduce all the experimental fluctuation data for the echinocyte, the stomatocyte, and, although in a limited range of q only, for the discocytes. The model assumes a homogeneous bilayer; we therefore propose that the spectrin networks of the echinocyte and the stomatocyte have a regular structure since the continuum model applies for these cells. Irregularities in the spectrin cytoskeleton of the discocytes might lead to local fluctuations whose description is beyond the scope of the model presented here.

The echinocyte has little ATP, a strongly connected cytoskeleton with few defects, and—according to our analysis—can be fit with no need to account for active effects. The stomatocyte has an abundance of ATP and a high effective temperature and shows strong active effects. A large amount of ATP might lead to a weak cytoskeleton with many defects and a low value of μ [39,75]. The cytoskeleton of the echinocyte, which has little ATP, may be idealized as an hexagonal lattice. On the other hand, the discocyte that has significant ATP may show many defects and larger "holes" in its spectrin network. These defect regions may be responsible for the fact that our model cannot fit the discocyte data for $q \gtrsim 0.008\ \text{nm}^{-1}$. The skeleton of the stomatocyte, with even more ATP than the discocyte, may have so many ATP-induced defects that the cytoskeleton behaves almost as a uniform amorphous network [86] and that there are no longer any strong inhomogeneities. This interpretation is consistent with our fits using the continuum model, but with different values of the parameters.

Our model describes the fluctuation spectrum at wave vectors $q \lesssim 0.008\ \text{nm}^{-1}$ with elastic parameters that are similar to those found in other experiments. At these small wave vectors, the shear modulus obtained from the fluctuation experiments is even larger than the values found in many static deformation experiments. The larger values of μ compared to values obtained by static deformations might be qualitatively explained by dynamic rearrangement of the cytoskeleton and strain softening [35,39,86,87]. The puzzle of an apparently very soft membrane, found in fluctuation measurements, and a stiff membrane, found in static deformation experiments, thus seems to be due to processes that mainly contribute to the spectrum at wave vectors $q \gtrsim 0.008\ \text{nm}^{-1}$.

An extended experimental study with several stomatocytes, discocytes, and echinocytes would be desirable. The evaluation of averages $\langle h(q_1)h(-q_2)\rangle$ with $q_1 \neq q_2$ could shed light on the nature of possible noncontinuum fluctuations at larger wave vectors, while a change of the viscosity of the buffer, starvation, or blocking of ATP processes could further clarify the role of active effects.

ACKNOWLEDGMENTS

We acknowledge helpful discussions with David Andelman, T. C. Lubensky, G. Gompper, J. Merath, J.-B. Fournier, P. Nelson, and A. Zemel. We thank G. Popescu for providing us with his unpublished data. This project has been supported by the EU Network Grant (SoftComp). T.A. thanks the Minerva Foundation. S.A.S. acknowledges support from the ISF and BSF as well as the Schmidt Minerva Center. N.G. thanks the Robert Rees Fund for Applied Research, the Alvin and Gertrude Levine Career Development Chair, and the Israel Science Foundation (Grant No. 337/05) for their support. This research was made possible in part by the historic generosity of the Harold Perlman Family.

APPENDIX A: DETAILS FOR COUPLED-MEMBRANE FLUCTUATIONS

The total free energy in Eq. (7) consists of (a) the free energy of the model Hamiltonian,

$$\mathcal{F}_0 = \frac{k_B T}{2} \sum_{\mathbf{q}} \ln[G_1(\mathbf{q}) G_2(\mathbf{q}) - G_m^2(\mathbf{q})] + c_{\mathcal{F}_0}, \tag{A1}$$

where $c_{\mathcal{F}_0}$ is independent of all propagators G_x; (b) the average over the model Hamiltonian, which is a constant; (c) the averages over the bending terms with respect to the model Hamiltonian,

$$\langle \mathcal{H}_1 \rangle_0 = \frac{1}{2} \sum_{\mathbf{q}} \kappa_1(\mathbf{q}) \mathbf{q}^4 \frac{G_2(\mathbf{q})}{G_1(\mathbf{q}) G_2(\mathbf{q}) - G_m^2(\mathbf{q})} \tag{A2}$$

and

$$\langle \mathcal{H}_2 \rangle_0 = \frac{1}{2} \sum_{\mathbf{q}} \kappa_s(\mathbf{q}) \mathbf{q}^4 \frac{G_1(\mathbf{q})}{G_1(\mathbf{q}) G_2(\mathbf{q}) - G_m^2(\mathbf{q})}; \tag{A3}$$

and (d) the interaction term

$$\langle \mathcal{H}_m \rangle_0 = \sqrt{2\pi} \upsilon_0 L^2 \frac{e^{-2\pi^2 d^2/\Delta^2}}{\Delta}, \tag{A4}$$

with $\Delta^2 = s_1 + s_2 + 2s_m$ and $s_x = (2\pi/L)^2 \Sigma_{\mathbf{q}} G_x(\mathbf{q}) / [G_1(\mathbf{q}) G_2(\mathbf{q}) - G_m^2(\mathbf{q})]$.

The total free energy in Eq. (7) is minimal at equilibrium; thus, its derivatives with respect to the three propagators need to vanish. The set of coupled equations

$$\begin{aligned} 0 = \frac{\partial \mathcal{F}}{\partial G_1(\mathbf{q})} = \frac{k_B T}{2} & \frac{G_2(\mathbf{q})}{G_1(\mathbf{q}) G_2(\mathbf{q}) - G_m^2(\mathbf{q})} \\ & - \frac{\mathbf{q}^4}{2} \frac{\kappa_1 G_2^2(\mathbf{q}) + \kappa_2 G_m^2(\mathbf{q})}{[G_1(\mathbf{q}) G_2(\mathbf{q}) - G_m^2(\mathbf{q})]^2} \\ & - \frac{\chi^{-4}}{2} \frac{G_2^2(\mathbf{q}) + G_m^2(\mathbf{q}) + 2 G_2(\mathbf{q}) G_m(\mathbf{q})}{[G_1(\mathbf{q}) G_2(\mathbf{q}) - G_m^2(\mathbf{q})]^2}, \end{aligned} \tag{A5}$$

$$\begin{aligned} 0 = \frac{\partial \mathcal{F}}{\partial G_2(\mathbf{q})} = \frac{k_B T}{2} & \frac{G_1(\mathbf{q})}{G_1(\mathbf{q}) G_2(\mathbf{q}) - G_m^2(\mathbf{q})} \\ & - \frac{\mathbf{q}^4}{2} \frac{\kappa_1 G_m^2(\mathbf{q}) + \kappa_2 G_1^2(\mathbf{q})}{[G_1(\mathbf{q}) G_2(\mathbf{q}) - G_m^2(\mathbf{q})]^2} \\ & - \frac{\chi^{-4}}{2} \frac{G_1^2(\mathbf{q}) + G_m^2(\mathbf{q}) + 2 G_1(\mathbf{q}) G_m(\mathbf{q})}{[G_1(\mathbf{q}) G_2(\mathbf{q}) - G_m^2(\mathbf{q})]^2}, \end{aligned} \tag{A6}$$

and

$$\begin{aligned} 0 = \frac{\partial \mathcal{F}}{\partial G_m(\mathbf{q})} = & - k_B T \frac{G_m(\mathbf{q})}{G_1(\mathbf{q}) G_2(\mathbf{q}) - G_m^2(\mathbf{q})} \\ & + \mathbf{q}^4 G_m(\mathbf{q}) \frac{\kappa_1 G_2(\mathbf{q}) + \kappa_2 G_1(\mathbf{q})}{[G_1(\mathbf{q}) G_2(\mathbf{q}) - G_m^2(\mathbf{q})]^2} \\ & + \chi^{-4} \frac{G_{12m}(\mathbf{q}) G_m(\mathbf{q}) + G_1(\mathbf{q}) G_2(\mathbf{q})}{[G_1(\mathbf{q}) G_2(\mathbf{q}) - G_m^2(\mathbf{q})]^2}. \end{aligned} \tag{A7}$$

where $G_{12m}(\mathbf{q}) = G_1(\mathbf{q}) + G_2(\mathbf{q}) + G_m(\mathbf{q})$ needs to be solved self-consistently, together with

$$\chi^{-4} = \upsilon_0 (2\pi)^{5/2} \frac{4\pi^2 d^2 - \Delta^2}{\Delta^5} e^{-2\pi^2 d^2/\Delta^2}. \tag{A8}$$

Equations (A5)–(A7) can be shown to reduce to

$$G_1(\mathbf{q}) = \frac{\kappa_1(\mathbf{q}) \mathbf{q}^4 + k_B T \chi^{-4}}{k_B T}, \tag{A9}$$

$$G_2(\mathbf{q}) = \frac{\kappa_2(\mathbf{q}) \mathbf{q}^4 + k_B T \chi^{-4}}{k_B T}, \tag{A10}$$

$$G_m(\mathbf{q}) = -\chi^{-4}. \tag{A11}$$

The limits for small and large χ^{-4} can be discussed in general for a coupling of membranes with arbitrary propagators. The effective propagators are

$$G_1(\mathbf{q}) = \frac{M_1(\mathbf{q}) + k_B T \chi^{-4}}{k_B T}, \tag{A12}$$

$$G_2(\mathbf{q}) = \frac{M_2(\mathbf{q}) + k_B T \chi^{-4}}{k_B T}, \tag{A13}$$

$$G_m(\mathbf{q}) = -\chi^{-4}, \tag{A14}$$

with the propagators of the independent membranes M_x. The expansions for small χ^{-4} are

$$\begin{aligned} \langle |h_1(\mathbf{q})|^2 \rangle = \left(\frac{L}{2\pi} \right)^2 \frac{k_B T}{M_1(\mathbf{q})} \Bigg[& 1 - \frac{1}{M_1(\mathbf{q})} \chi^{-4} \\ & + \frac{M_1(\mathbf{q}) + M_2(\mathbf{q})}{M_1^2(\mathbf{q}) M_2(\mathbf{q})} (\chi^{-4})^2 \Bigg], \end{aligned} \tag{A15}$$

$$\begin{aligned} \langle |h_2(\mathbf{q})|^2 \rangle = \left(\frac{L}{2\pi} \right)^2 \frac{k_B T}{M_2(\mathbf{q})} \Bigg[& 1 - \frac{1}{M_2(\mathbf{q})} \chi^{-4} \\ & + \frac{M_1(\mathbf{q}) + M_2(\mathbf{q})}{M_2^2(\mathbf{q}) M_1(\mathbf{q})} (\chi^{-4})^2 \Bigg], \end{aligned} \tag{A16}$$

$$\begin{aligned} \langle |h_2(\mathbf{q}) - h_1(\mathbf{q})|^2 \rangle = & \left(\frac{L}{2\pi} \right)^2 \frac{k_B T [M_1(\mathbf{q}) + M_2(\mathbf{q})]}{M_1(\mathbf{q}) M_2(\mathbf{q})} \\ & \times \Bigg[1 - \frac{M_1(\mathbf{q}) + M_2(\mathbf{q})}{M_1(\mathbf{q}) M_2(\mathbf{q})} \chi^{-4} \\ & + \frac{[M_1(\mathbf{q}) + M_2(\mathbf{q})]^2}{M_1^2(\mathbf{q}) M_2^2(\mathbf{q})} (\chi^{-4})^2 \Bigg], \end{aligned} \tag{A17}$$

up to second order in χ^{-4}. The expansions for large χ^{-4} are

$$\begin{aligned} \langle |h_1(\mathbf{q})|^2 \rangle = \left(\frac{L}{2\pi} \right)^2 \frac{k_B T}{M_1(\mathbf{q}) + M_2(\mathbf{q})} \Bigg[& 1 + \frac{M_2^2(\mathbf{q})}{M_1(\mathbf{q}) + M_2(\mathbf{q})} \frac{1}{\chi^{-4}} \\ & - \frac{M_2^3(\mathbf{q}) M_1(\mathbf{q})}{[M_1(\mathbf{q}) + M_2(\mathbf{q})]^2} \frac{1}{(\chi^{-4})^2} \Bigg], \end{aligned} \tag{A18}$$

$$\langle |h_2(\mathbf{q})|^2 \rangle = \left(\frac{L}{2\pi}\right)^2 \frac{k_B T}{M_1(\mathbf{q}) + M_2(\mathbf{q})} \left[1 + \frac{M_1^2(\mathbf{q})}{M_1(\mathbf{q}) + M_2(\mathbf{q})} \frac{1}{\chi^{-4}} - \frac{M_1^3(\mathbf{q}) M_2(\mathbf{q})}{[M_1(\mathbf{q}) + M_2(\mathbf{q})]^2} \frac{1}{(\chi^{-4})^2} \right], \tag{A19}$$

$$\langle |h_2(\mathbf{q}) - h_1(\mathbf{q})|^2 \rangle = \left(\frac{L}{2\pi}\right)^2 k_B T \left[\frac{1}{\chi^{-4}} - \frac{M_1(\mathbf{q}) M_2(\mathbf{q})}{M_1(\mathbf{q}) + M_2(\mathbf{q})} \frac{1}{(\chi^{-4})^2} \right], \tag{A20}$$

up to second order in χ^4.

APPENDIX B: EFFECTIVE BENDING RIGIDITY FOR SOLID MEMBRANES

In this appendix, details of the renormalization of the bending rigidity of a nearly planar solid membrane and an effective fluctuation potential that occurs for solid membranes with an average local curvature are presented. The discussion is based on Refs. [51,53,54].

1. Shear-bending renormalization for almost planar membranes

The fluctuations of a nearly flat solid membrane can be described at large wave vectors by a wave-vector-independent bending rigidity. The interaction between bending and shear modes leads to a renormalization of the wave-vector-independent bending rigidity that increases the effective bending rigidity at small wave vectors [53,54],

$$\kappa_R(\mathbf{q}) = \kappa_c + K_0 k_B T \int \frac{d^2\mathbf{k}}{(2\pi)^2} \frac{[\hat{q}_i P_{ij}(\mathbf{k}) \hat{q}_j]^2}{\kappa |\mathbf{k} + \mathbf{q}|^4}. \tag{B1}$$

The projection operator $P_{ij}(\mathbf{k}) = \delta_{ij} - k_i k_j / k^2$ is $P_{xx} = 1 - k_x^2/k^2$ for $\hat{q}_i = \hat{q}_j = \hat{q}_x$. The renormalized bending rigidity in x direction is

$$\kappa_R(\mathbf{q}) = \kappa_c + \frac{K_0 k_B T}{(2\pi)^2} \int_0^\infty dk \int_0^{2\pi} d\Theta \frac{k(1 - \cos^2\Theta)^2}{\kappa(k^2 + q^2 + 2kq\cos\Theta)^2}. \tag{B2}$$

In the limit of small q, κ_R in Eq. (B1) can be calculated self-consistently using the assumption $\kappa_R = \kappa = \alpha_r q^{-1}$ and $\kappa_c = 0$. We obtain [55]

$$\alpha_r q^{-1} = \sqrt{\frac{k_B T K_0}{4\pi}} \frac{1}{\mathbf{q}}. \tag{B3}$$

For large q, we use $\kappa = \kappa_c$ (which is independent of q) in the integral in Eq. (B2). After substituting $y = k/q$, we evaluate the integral and obtain the perturbative result for the shear-bending interaction:

$$\kappa_R(\mathbf{q}) = \kappa_c + \frac{3 k_B T K_0}{16\pi\kappa_c} \frac{1}{\mathbf{q}^2}. \tag{B4}$$

In both equations, the bulk compression modulus K_0 is [51]

$$K_0 = \frac{4\mu(\mu + \lambda)}{2\mu + \lambda}, \tag{B5}$$

where $\lambda = -2\mu\nu/(\nu - 1)$. If the area is fixed (e.g., if a polymer network is attached to a lipid bilayer), $\nu = 1/2$ and $K_0 = 3\mu$. For a free polymer network, $\nu = -1/3$ [6] and $K_0 = 4\mu/3$.

2. Confinement potential for a membrane with shear that has a nonzero average curvature

For a membrane with shear elasticity, the fluctuation behavior differs considerably depending whether the average membrane shape is curved or planar. If the average membrane shape is planar, only the wave-vector-independent bending term or the renormalized bending rigidity due to the interaction between bending and shear modes contributes. If the average membrane shape is curved, an additional confinement potential contribution appears.

The free energy to stretch a membrane with shear elasticity can be written as integral over the membrane area S [51],

$$\mathcal{F}_\mathrm{p} = \frac{h_s}{2} \int_S dS u_{\alpha\beta} \sigma_{\alpha\beta}. \tag{B6}$$

The thickness of the solid membrane, h_s, the deformation tensor $u_{\alpha\beta}$, and the stress tensor $\sigma_{\alpha\beta}$ enter the integral. The stress tensor is given by

$$\sigma_{\alpha\beta} = \frac{E}{1 - \nu^2} [(1 - \nu) u_{\alpha\beta} + \nu \delta_{\alpha\beta} u_{\gamma\gamma}], \tag{B7}$$

with Young modulus E and the Poisson ratio ν.

In order to calculate the confinement potential, the stretching contributions due to a homogeneous increase h of the radii of a sphere and a cylinder with radii R are calculated. Only in-plane stretching can balance the forces of increased radii. Thus the nonzero components for the stretching tensor for a sphere are $u_{\theta\theta} = h/R$ and $u_{\phi\phi} = h/R$, and for a cylinder, $u_{\phi\phi} = h/R$. The stretching energies for sphere and cylinder become

$$\mathcal{F}_\mathrm{p,sph} = \frac{E h_s}{1 - \nu^2} \int dS \left(\frac{h}{R}\right)^2 \tag{B8}$$

and

$$\mathcal{F}_\mathrm{p,cyl} = \frac{E h_s}{2(1 - \nu^2)} \int dS \left(\frac{h}{R}\right)^2 \tag{B9}$$

respectively. Expressed in terms of mean curvature $H = (c_1 + c_2)/2$ and Gaussian curvature $K = c_1 c_2$, where c_1 and c_2 are the two principal curvatures, the potential term in the Hamiltonian is

$$\mathcal{H}_\mathrm{p} = \frac{E h_s}{1 - \nu^2} \int dS (2H^2 - K) h^2 \tag{B10}$$

$$= \left[4\mu \int dS (2H^2 - K) \right] h^2, \tag{B11}$$

where $\mu = E h_s / 2/(1 + \nu)$ and $\nu = 1/2$ have been used.

APPENDIX C: INTERACTION LENGTH χ, CHARACTERISTIC WAVE VECTOR $\tilde{q}$, AND CROSSOVER WAVE VECTOR q^+

The confinement potential term due to the excluded-volume interaction, $k_BT\chi^{-4}$, and thus the interaction length χ, as well as a characteristic wave vector $\tilde{q}$, can be estimated for the fluid-fluid and the solid-solid system by extension of Helfrich's original argument for one fluid membrane between two walls [8]. The sum of the mean-squared fluctuation amplitudes of both membranes must cover the available volume, so that

$$\langle h_1^2(r)\rangle + \langle h_2^2(r)\rangle = \xi d^2, \tag{C1}$$

with ξ a number of the order of unity, but $\xi < 1$. An ansatz in which an excluded-volume potential τ is added to each propagator,

$$\frac{1}{4\pi^2}\int_0^\infty d\mathbf{q}\left[\frac{k_BT}{\kappa_1 q^4 + \tau_1} + \frac{k_BT}{\kappa_2 q^4 + \tau_2}\right] = \xi d^2, \tag{C2}$$

is used to restrict fluctuation amplitudes subject to the constraint of Eq. (C1) [88]. When both membranes are identical, $\kappa = \kappa_1 = \kappa_2$ and $\tau = \tau_1 = \tau_2$, the confinement potential can be expressed through a characteristic wave vector $\tilde{q}$. In the case of two fluid membranes, $\tau = \tilde{q}^4\kappa_f$, and in the case of two solid membranes, $\tau = \tilde{q}^3\alpha_r$. The physical meaning of $\tilde{q}$ is to characterize the typical in-plane distance between interactions of the membranes.

In the limit $v_0 \to \infty$, only one energy and one length enter the equations. Thus all lengths in this subsection, χ, $1/\tilde{q}$, and $1/q^+$, show the same scaling with κ_f, μ, and d. Because of the different definitions of these physical quantities, the prefactors differ.

For two fluid membranes—i.e., $\kappa = \kappa_f$—the result derived by Helfrich is

$$\tilde{q} = \frac{1}{2}\sqrt{\frac{k_BT}{\kappa_f\xi}}\frac{1}{d}. \tag{C3}$$

The characteristic wave vector increases for smaller d as well as for smaller κ_f. The corresponding interaction length is

$$\chi = \left(\frac{k_BT}{\tau}\right)^{1/4} = \left(\frac{k_BT}{\kappa_f\tilde{q}^4}\right)^{1/4} = \frac{2\xi^{1/2}\kappa_f^{1/4}d}{(k_BT)^{1/4}}. \tag{C4}$$

For two solid membranes, we obtain from Eq. (C2)

$$\tilde{q} = \frac{2}{3\sqrt{3}}\frac{k_BT}{\alpha_r\xi d^2} = \frac{4\sqrt{\pi}}{9}\frac{\sqrt{k_BT}}{\xi d^2\sqrt{\mu}}. \tag{C5}$$

The corresponding interaction length is

$$\chi = \left(\frac{k_BT}{\tau}\right)^{1/4} = \left(\frac{k_BT}{\alpha_r\tilde{q}^3}\right)^{1/4} \sim d^{3/2}\mu^{1/4}. \tag{C6}$$

In Fig. 7, we see that the predicted scaling behaviors for both fluid and solid membranes are reproduced by our more microscopic model described in Sec. II. The scaling exponents obtained by numerical solution of our model [Eqs. (9)–(11) and Δ given after Eq. (A4)] are slightly smaller than those expected from simple scaling where the only energy and length scales in the system are κ (or μ) and d. Our theory, which includes an additional length scale associated with the excluded volume, approaches the values obtained by simple scaling in the limit $v_0 \to \infty$. The free energy for the solid membranes scales like d^{-4}, and the free energy for the fluid membranes scales like d^{-2}; both increase strongly at small d. Since the strength of the contact interaction, v_0, is finite, at small enough d the membranes will significantly interpenetrate. This leads to a modification of the scaling, which is clearly visible for the solid membranes in Fig. 7.

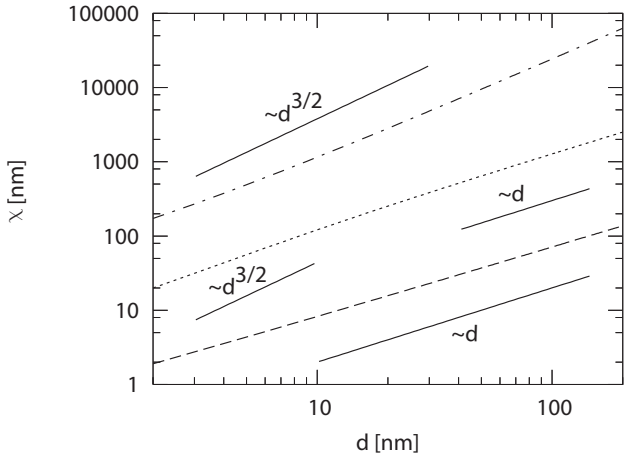

FIG. 7. Interaction distance χ as a function of d for different systems: two fluid membranes with $\kappa_f = 3k_BT$ (dashed line), two solid membranes with $\mu = 30k_BT$ nm^{-2} (dash-dotted line), one solid and one fluid membrane with $\kappa_f = 30k_BT$ and $\mu = 30k_BT$ nm^{-2} (dotted line). In all cases, $v_0 = 1k_BT$ nm^{-1}. The numerical result for the solid membranes has been multiplied by 100, the result for the fluid-solid membrane pair by 10. For the fluid-solid system, a crossover from the solidlike scaling at small d to the fluidlike scaling at large d is observed.

For the numerical result of the fluid-solid membrane pair, a crossover is observed between the solidlike scaling of χ at small d where $\chi \sim d^{3/2}$ and fluidlike scaling at large d where $\chi \sim d$. At small d, coherent long-wavelength fluctuations are suppressed. The bending modulus of the solid membrane for small-wavelength fluctuations is small and the fluid membrane is stiff compared with the solid membrane. The system acts like a solid membrane next to a planar wall. At large d, coherent long-wavelength fluctuations are permitted with a consequent strong renormalization of the bending modulus of the solid membrane. The solid membrane is stiff compared to the fluid membrane; the system acts like a fluid membrane next to a planar wall. This crossover is further discussed in Sec. IV.

Consequently, for a fluid-solid system at a fixed spacing, either fluid and solid scaling can be obtained for different values of the elastic parameters. A large shear term and a small bending term leads to fluidlike scaling behavior for the interaction length χ, while a large bending term and a small shear term leads to solidlike scaling behavior. If the rescaled numerical results for several values of κ and μ are plotted as a function of d/d^* (d^* defined in Sec. IV), the crossover in the slope for $d < d^*$ and $d > d^*$ is clearly visible; see Fig. 8.

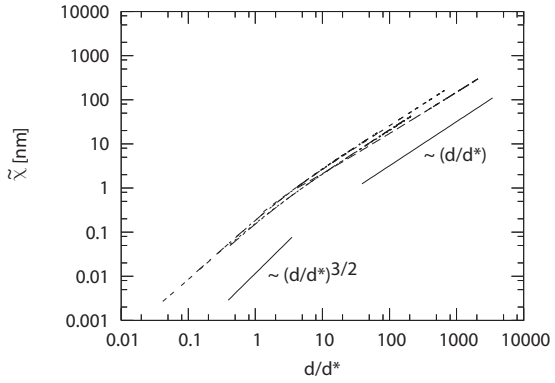

FIG. 8. Interaction parameter as function of d/d^*, where d^* is the crossover between fluid and solid scaling upon changes of d. The χ values have been rescaled in order to allow easy comparison of the slopes. All numerical results are for $v_0=10^3 k_B T$ nm^{-1}, unscaled distances $2 \leqslant d \leqslant 1000$nm, and membrane pairs with $\mu_1=3k_BT$ nm^{-1} and $\kappa_1=300k_BT$ ($d_1^*=48$nm), $\mu_2=30k_BT$ nm^{-1} and $\kappa_2=300k_BT$ ($d_2^*=15$nm), $\mu_3=30k_BT$ nm^{-1} and $\kappa_3=30k_BT$ ($d_3^*=4.8$nm), $\mu_4=3k_BT$ nm^{-1} and $\kappa_4=3k_BT$ ($d_4^*=4.8$nm), $\mu_5=300k_BT$ nm^{-1} and $\kappa_5=30k_BT$ ($d_5^*=1.5$nm), and $\mu_6=300k_BT$ nm^{-1} and $\kappa_6=3k_BT$ ($d_6^*=0.5$nm).

The scaling $\tilde{\chi} \sim d/d^*$ and $\tilde{\chi} \sim (d/d^*)^{3/2}$ follows from Eqs. (C4) and (C6), respectively.

The wave vector that characterizes the crossover between coupled and uncoupled fluctuations of both membranes, q^+, can be estimated by calculating the conditions under which the ratio of the mean squared fluctuations of the distance of both membranes compared with the relative mean squared fluctuations of the distance of two non-interacting membranes is of order unity (here taken to be 1/2):

$$\frac{1}{2} = \frac{\langle |h_2(q^+) - h_1(q^+)|^2 \rangle}{\langle |h_2(q^+) - h_1(q^+)|^2 \rangle_\infty}. \tag{C7}$$

The index ∞ indicates the limit $d \to \infty$ when the membranes do not interact. In that case, the distance fluctuations of the non-interacting membranes are given by the sum of the mean squared fluctuation amplitudes of both membranes. This sum is always finite and becomes larger when the values of the elastic constants decrease—whereas the numerator of the right-hand side of Eq. (C7) decreases for smaller values of the elastic constants [see Eq. (13) and discussion thereafter].

APPENDIX D: FREE ENERGY PER MEMBRANE AREA

The differences between the free energy per unit area for finite values of d and for free membranes ($d \to \infty$) can be derived using scaling arguments,

$$\Delta f_f \sim \frac{(k_B T)^2}{\kappa_f \xi d^2} \tag{D1}$$

for the fluid membranes and

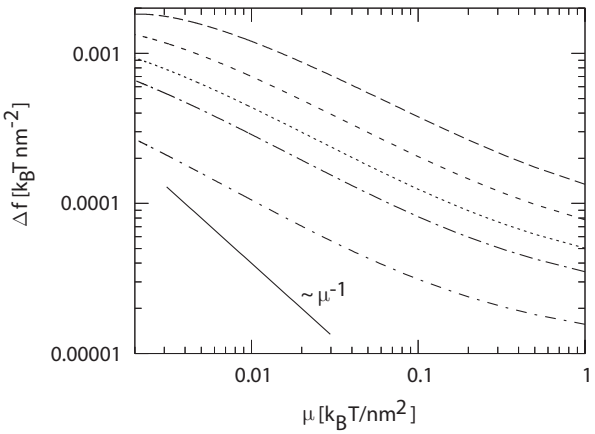

FIG. 9. Free energy difference per unit area between the composite membrane and the sum of the free energies of the noninteracting membranes for $v_0=0.1k_BT$ nm^{-1} and several values of d (from top to bottom: $d=20,25,30,35,50$ nm). The numerical results are plotted as function of μ using $\kappa_f=10k_BT$. Larger values of κ_f decrease the free energy differences for small values of μ. Slopes that are closer to the expected scaling of a polymerized membrane, $\Delta f \sim \mu^{-1}$ [Eq. (D2)], are obtained for larger values of v_0 and small values of μ.

$$\Delta f_s \sim \frac{(k_B T)^2}{\mu \xi^2 d^4} \tag{D2}$$

for the solid membranes [7]. To calculate the d dependence of the free energy and, hence, of the repulsive pressure between the membranes with the coupled membrane model, Eqs. (9)–(11) must be solved self-consistently. Using Eq. (7), the difference between the free energy of the interacting membranes and the free energy of two non-interacting membranes ($d \to \infty$) can then be evaluated numerically. For a bending rigidity $\kappa_f=10k_BT$, an interaction parameter $v_0=0.1k_BT$ nm^{-1}, and several values of d, the free energy differences per membrane area are plotted as a function of μ in Fig. 9. The parameters chosen are appropriate for the red blood cell membrane [18,32–35,62–65]. In the context of the red blood cell, this figure thus shows the influence of the degrees of freedom of the spectrin network on the dependence of the free energy on the bilayer-spectrin spacing and, hence, the interactions [89]. The fluctuating membrane approach is an extension of models in which the spectrin is considered as a hard wall that only restricts the bilayer fluctuations; see, e.g., Ref. [25].

For the distances $d=30$, 35, and 50 nm, a clear crossover in the free energy as function of μ can be observed. As discussed above, for large shear moduli the fluid behavior dominates; Δf depends only marginally on μ, since the solid membrane acts like a hard wall. For small shear moduli, fluctuations of the solid membrane dominate; $\Delta f \sim \mu^{-1}$ is expected for simple scaling and two solid membranes. In Fig. 9, the observed scaling exponent is larger than -1, due to the finite values of v_0 and κ_f. The decreasing slope of Δf for large μ indicates the increasing importance of the fluctuations of the fluid and the decreasing importance of the

fluctuations of the solid membrane. Variations of κ_f (not shown in Fig. 9) mainly affect the values of Δf for large μ [Eq. (C3)]. At very large values of μ, the solid membrane hardly fluctuates; the fluctuation free energy arises from the fluctuations of the fluid membrane and is thus independent of μ. Since κ_f enters the free energy in the denominator [Eq. (D1)], a larger value lowers the free energy difference Δf and, hence, the interactions.

APPENDIX E: COUPLED MEMBRANE MODEL vs SINGLE EFFECTIVE MEMBRANE, CHOICE OF EFFECTIVE BENDING RIGIDITY

For the RBC, the fluctuations of the spectrin cytoskeleton at the wave vectors measured in the experimental data are in a regime where the shear-bending renormalization of the spectrin bending modulus is significant and Eq. (19) applies. In addition, since the membrane of the RBC has an average mean curvature of the order 4×10^{-4} nm^{-1}, the confinement potential term in Eq. (21) must be added to further constrain the fluctuations.

We now compare the coupled membrane model in the two regimes of self-consistent and perturbative shear-bending interaction with the experimental data. The mean-squared fluctuation amplitudes $\langle|h(q)|^2\rangle=k_BT/(\kappa(q)q^4)$ of both experiment and theory are normalized by the fluctuation amplitudes of a noninteracting fluid membrane, $\langle|h_{25}(q)|^2\rangle=1/(25q^4)$, where the subscript 25 refers to our choice of $\kappa=25k_BT$, which is a reasonable value for a lipid membrane [18,62–64,90]. The normalization emphasizes the data at large q and highlights a sudden increase of the fluctuation amplitudes at $q\approx0.008$ nm^{-1} [25]. In the theory, we estimate that because of the relatively large mesh size (compared with the lipid spacing), the constant bending rigidity of the spectrin network is small, $\kappa_c\approx0.1k_BT$ [25]. The average cell shapes, needed to determine the potential strengths γ, are taken from Ref. [69].

The theoretical estimate of the crossover wave vector for the shear-bending renormalization of the spectrin network alone is $q^*\approx0.07$ nm^{-1}, which is well above the wave vectors of the experimental data, $q<0.015$ nm^{-1} [91]. We are thus in a regime where the bending modulus of the spectrin layer is strongly renormalized and use the effective bending rigidity $\alpha_r q^{-1}+\gamma q^{-4}$ for the spectrin layer, and a constant bending rigidity κ_b for the bilayer. From the fit with the coupled membrane model to the experimental data at small q, we obtain $\kappa_b=4k_BT$ and $\mu=1.4\times10^{-2}k_BT$ nm^{-2} [66]; see Fig. 10. Both values of the fit parameters are subject to uncertainties. The value of μ depends on the shape of the cell which is not exactly known for the cell under consideration and the average over the entire cell area to obtain γ is certainly approximate. More importantly, experimental measurements of the fluctuation spectrum are usually based on a rectangular section of the cell surface and not on the entire area of the cell. The estimate of κ_b in our fit suffers from the lack of data points at large q; the largest value of κ_b that still fits the experiment up to the jump has been chosen [92].

In Fig. 10, the fluctuation spectrum of the coupled membrane model is compared with the spectrum of a single effective membrane, $\langle h(q)^2\rangle=k_BT/[\kappa_1(q)q^4]$, with bending rigidity $\kappa_1(q)=\kappa_b+\alpha_r q^{-1}+\gamma q^{-4}$, using the same elastic constants as derived from the fit discussed in the last paragraph. In the range of the experimental data, the two models (coupled membranes and single effective membrane) are indistinguishable, since the fluctuations of the bilayer and the cytoskeleton are strongly coupled. Because of the strong coupling, the fluctuation spectrum is insensitive to the exact values of v_0 and d. Thus, the finite spacing and individuality of each membrane, bilayer and spectrin, cannot account for the jump observed in the experimental data. Furthermore, since the coupling by a homogeneous pressure that maintains the average spacing of both layers is a smaller coupling compared to coupling by real anchor proteins (which leads in a continuum approach to the same value of d), we conclude that effects due to discrete, periodic coupling cannot explain the sudden increase of the fluctuation amplitudes.

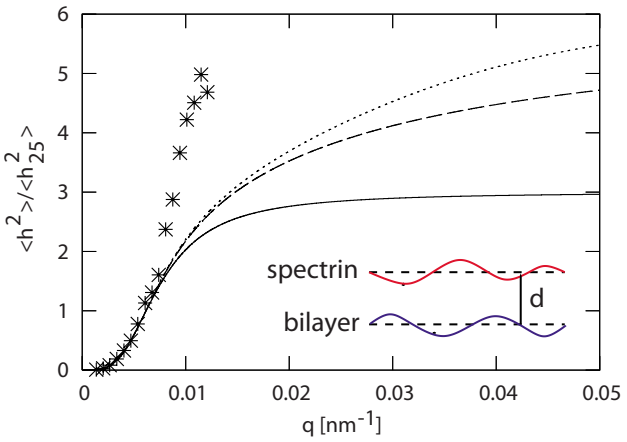

FIG. 10. (Color online) Discocyte fluctuation data of Ref. [36] and theoretical models. The experimental fluctuation amplitudes are normalized by the fluctuation amplitudes of a free membrane with $\kappa=25k_BT$, $\langle h_{25}^2\rangle$. The coupled membrane model (dotted line), a *single* membrane with an effective bending rigidity $\kappa_1(q)=\kappa_b+\alpha_r q^{-1}+\gamma q^{-4}$ (dashed line), and a *single* membrane with an effective bending rigidity $\kappa_2(q)=\kappa_b+\alpha_p q^{-2}+\gamma q^{-4}$ (solid line). In the inset, our model of two membranes that fluctuate at fixed spacing d is sketched.

For strongly coupled membranes, the constant bending rigidity that should now be used to calculate q^* is the bending rigidity of the lipid bilayer, κ_b, instead of the bare spectrin bending modulus κ_c. When this is done, the value of q^* decreases significantly and the single effective membrane is no longer in the regime where the shear modes strongly renormalize the bending modes. Thus, the perturbative term $\alpha_p q^{-2}$ seems more appropriate for the renormalization of the spectrin bending modulus than the $\alpha_r q^{-1}$ term used earlier. Since we do not know *a priori* the value of the elastic constants obtained with the perturbative term, we also fit the experimental data using an effective, single membrane with bending modulus $\kappa_2(q)=\kappa_b+\alpha_p q^{-2}+\gamma q^{-4}$. We now obtain $\kappa_b=8k_BT$ and $\mu=1.2\times10^{-2}k_BT$ nm^{-2}. (The discrepancy between the small values of κ_b found in the fits and the value $\kappa_b=25k_BT$ expected for a typical lipid membrane is discussed in Sec. V C in terms of ATP activity [93].)

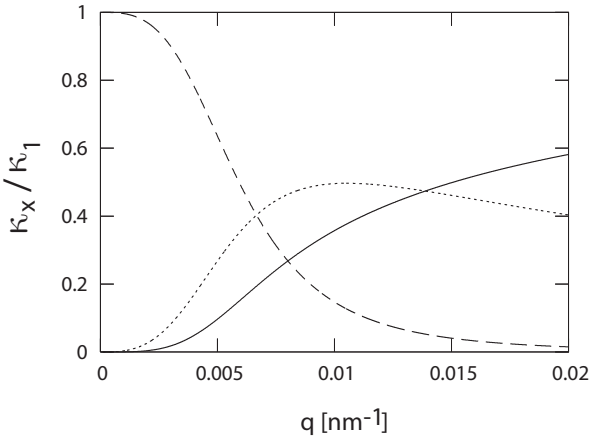

FIG. 11. Relative contributions of the constant bending rigidity κ_b (solid line), the shear contribution $\alpha_r q^{-1}$ (dotted line), and the potential term γq^{-4} (dashed line) to the total effective bending modulus $\kappa_1(q)=\kappa_b+\alpha_r q^{-1}+\gamma q^{-4}$.

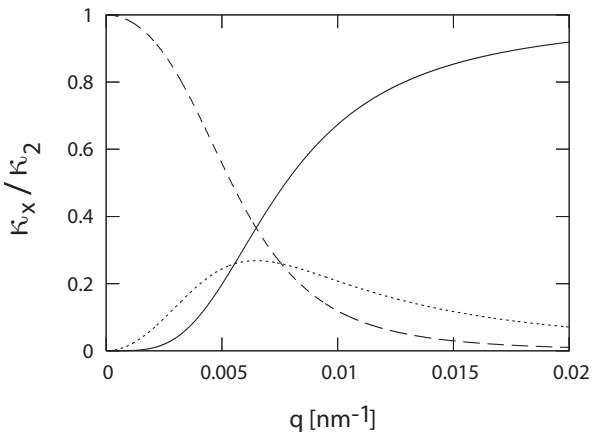

FIG. 12. Relative contributions of the constant bending rigidity κ_b (solid line), the shear contribution $\alpha_p q^{-2}$ (dotted line), and the potential term γq^{-4} (dashed line) to the total effective bending modulus $\kappa_2(q)=\kappa_b+\alpha_p q^{-2}+\gamma q^{-4}$.

Both approaches, the self-consistent, $\kappa_1(q)$, as well as the perturbative, $\kappa_2(q)$, agree with the low-q data, shown in Fig. 10. The values of the shear moduli found in both fits are similar, but the fitted values of the bending moduli of the lipid bilayer differ by a factor of 2. To decide which fit to use, we compare the relative contributions to the effective bending rigidities in both cases, shown in Figs. 11 and 12. The strong dominance of the potential term γq^{-4} at small q results in similar values of the shear moduli in the fits with either $\kappa_1(q)$ or $\kappa_2(q)$. Figure 11 shows the crossover between $\alpha_r q^{-1}$ and κ_b in the range of the wave vectors of interest. We see that the use of $\alpha_r q^{-1}$ is not justified, because for the derivation of this contribution it has been assumed that the renormalized bending rigidity $\alpha_r q^{-1}$ is *much* larger than the constant contribution to the bending rigidity. This is not the case in Fig. 11. In Fig. 12, it is shown that the perturbative contribution to $\kappa_2(q)$, $\alpha_p q^{-2}$, never accounts for more than 30% to the total bending modulus. This indicates that the perturbation approach is consistent and that $\kappa_2(q)$ is more appropriate than $\kappa_1(q)$.

The perturbation theory $\kappa_2(q)$ is consistent and appears more appropriate than the self-consistent theory $\kappa_1(q)$. We use the perturbation result to analyze the fluctuation data for several cells in Secs. V B and V C. The perturbative term in $\kappa_2(q)$, arising from the coupling of the shear and bending modes, gives an alternative physical origin for the large surface tension term used in the fits in Ref. [25] and is indeed much larger than the small tension that arises from the constraint of finite area due to the closed shape of the cell.

[1] W. Helfrich, Z. Naturforsch. C **28**, 693 (1973).
[2] H. G. Dobereiner, G. Gompper, C. K. Haluska, D. M. Kroll, P. G. Petrov, and K. A. Riske, Phys. Rev. Lett. **91**, 048301 (2003).
[3] W. K. den Otter and W. J. Briels, J. Chem. Phys. **118**, 4712 (2003).
[4] F. F. Abraham and D. R. Nelson, J. Phys. (Paris) **51**, 2653 (1990).
[5] J. Aronovitz, L. Golubovic, and T. C. Lubensky, J. Phys. (Paris) **50**, 609 (1989).
[6] G. Gompper and D. M. Kroll, Curr. Opin. Colloid Interface Sci. **2**, 373 (1997).
[7] S. A. Safran, *Statistical Thermodynamics of Surfaces, Interfaces, and Membranes* (Addison-Weasley, Reading, MA, 1994).
[8] W. Helfrich, Z. Naturforsch. A **33**, 305 (1978).
[9] G. Gompper and D. M. Kroll, Europhys. Lett. **9**, 59 (1989).
[10] R. Lipowsky, Europhys. Lett. **7**, 255 (1988).
[11] G. Gompper and D. M. Kroll, J. Phys. I (Paris) **1**, 1411 (1991).
[12] G. Gompper and D. M. Kroll, Europhys. Lett. **15**, 783 (1991).
[13] M. O. Robbins, D. Andelman, and J. F. Joanny, Phys. Rev. A **43**, 4344 (1991).
[14] P. S. Swain and D. Andelman, Langmuir **15**, 8902 (1999).
[15] P. S. Swain and D. Andelman, Phys. Rev. E **63**, 051911 (2001).
[16] R. J. Merath and U. Seifert, Phys. Rev. E **73**, 010401(R) (2006).
[17] In the long-wavelength, strong-coupling regime, the membranes show relatively small fluctuations in their separation. Large fluctuations in the intermembrane distance would give rise to a large increase in the excluded-volume repulsions (due to fluctuations at shorter wavelengths) and raise the free energy. This is true even though in other regions the two membranes would be separated to distances much larger than the average spacing, since the repulsion varies as $1/d^n$ where n is equal to 2 or larger; this gives more weight to the regions in which the membranes are locally closely spaced. The upshot is that the two membranes fluctuate as a single, composite membrane at the large wavelengths where the strong-coupling regime applies.

[18] H. Noguchi and G. Gompper, Proc. Natl. Acad. Sci. U.S.A. **102**, 14159 (2005).

[19] G. M. Artmann, C. Kelemen, D. Porst, G. Buldt, and S. Chien, Biophys. J. **75**, 3179 (1998).

[20] D. D. Lasic, Angew. Chem., Int. Ed. Engl. **33**, 1685 (1994).

[21] J. C. Hansen, R. Skalak, S. Chien, and A. Hoger, Biophys. J. **72**, 2369 (1997).

[22] E. Sackmann, Can. J. Phys. **68**, 999 (1990).

[23] M. P. Sheetz, J. E. Sable, and H. G. Dobereiner, Annu. Rev. Biophys. Biomol. Struct. **35**, 417 (2006).

[24] A. Zidovska and E. Sackmann, Phys. Rev. Lett. **96**, 048103 (2006).

[25] N. Gov, A. G. Zilman, and S. Safran, Phys. Rev. Lett. **90**, 228101 (2003).

[26] J. B. Fournier, D. Lacoste, and E. Raphael, Phys. Rev. Lett. **92**, 018102 (2004).

[27] S. B. Rochal and V. L. Lorman, Phys. Rev. Lett. **96**, 248102 (2006).

[28] D. H. Boal, U. Seifert, and A. Zilker, Phys. Rev. Lett. **69**, 3405 (1992).

[29] H. W. G. Lim, M. Wortis, and R. Mukhopadhyay, Proc. Natl. Acad. Sci. U.S.A. **99**, 16766 (2002).

[30] F. Brochard and J. F. Lennon, J. Phys. (Paris) **36**, 1035 (1975).

[31] An approach to unravel the puzzle of a high shear stiffness but yet a floppy membrane is presented in Ref. [28]. Tethers of finite length that represent the spectrin molecules might allow for small bilayer fluctuations but not for large-scale deformations in micromechanical experiments. To obtain this nonlinear behavior of the network with respect to shear distortions, it has to be assumed that the spectrin tethers can be expanded to a certain length with almost no cost of energy. This model is not consistent with approaches that treat the spectrin cytoskeleton as a network of springs [21,39,86].

[32] R. M. Hochmuth, J. Biomech. Eng. **115**, 515 (1993).

[33] E. A. Evans, Methods Enzymol. **173**, 3 (1989).

[34] J. Guck, R. Ananthakrishnan, H. Mahmood, T. J. Moon, C. C. Cunningham, and J. Kas, Biophys. J. **81**, 767 (2001).

[35] J. C. M. Lee and D. E. Discher, Biophys. J. **81**, 3178 (2001).

[36] A. Zilker, H. Engelhardt, and E. Sackmann, J. Phys. (Paris) **48**, 2139 (1987).

[37] G. Popescu, T. Ikeda, K. Goda, C. A. Best-Popescu, M. Laposata, S. Manley, R. R. Dasari, K. Badizadegan, and M. S. Feld, Phys. Rev. Lett. **97**, 218101 (2006).

[38] S. Tuvia, S. Levin, A. Bitler, and R. Korenstein, J. Cell Biol. **141**, 1551 (1998).

[39] N. S. Gov and S. A. Safran, Biophys. J. **88**, 1859 (2005).

[40] J. Palek and P. Jarolim, Semin Hematol. **30**, 249 (1993).

[41] J. A. Ursitti and J. B. Wade, Cell Motil. Cytoskeleton **25**, 30 (1993).

[42] B. S. Bull, R. S. Weinstein, and R. A. Korpman, Blood Cells **12**, 25 (1986).

[43] V. Heinrich, K. Ritchie, N. Mohandas, and E. Evans, Biophys. J. **81**, 1452 (2001).

[44] G. Popescu, T. Ikeda, C. A. Best, K. Badizadegan, R. R. Dasari, and M. S. Feld, J. Biomed. Opt. Lett. **10**, 060503 (2005).

[45] Our model applies not only to fluid and solid membranes, but also to membranes with any kind of effective bending moduli—e.g., polymer-decorated membranes [81,82].

[46] $G_m^2(\mathbf{q}) > G_1(\mathbf{q})G_2(\mathbf{q})$ limits the applicability of the model.

[47] M. Doi and S. F. Edwards, *The Theory of Polymer Dynamics*, 1st ed. (Clarendon Press, Oxford, 1986).

[48] Since we want to constrain the distance d between the membranes, fluctuations that involve $q=0$ correspond to translations of the center of mass of each membrane are not allowed.

[49] A calculation that uses this approach for interface fluctuations in binary liquid mixtures is found in Ref. [50].

[50] T. Hiester, S. Dietrich, and K. Mecke, J. Chem. Phys. **125**, 184701 (2006).

[51] L. D. Landau and E. M. Lifshitz, *Theory of Elasticity*, 3rd ed. (Pergamon Press, Oxford, 1986).

[52] Lipid membranes are thinner but have distances between the lipids that are much smaller than the polymer bond lengths b.

[53] D. R. Nelson, *Defects and Geometry in Condensed Matter Physics*, 1st ed. (Cambridge University Press, Cambridge, England, 2002).

[54] D. R. Nelson and L. Peliti, J. Phys. (Paris) **48**, 1085 (1987).

[55] The "q^{-1} renormalization" obtained by a simple self-consistent calculation has been shown by computer simulations and more sophisticated analytical calculations to depend on the wave vector as $q^{-0.82}$. For this paper, the small difference in the exponent is not relevant.

[56] M. A. Peterson, J. Math. Phys. **26**, 711 (1985).

[57] U. Seifert, Adv. Phys. **46**, 13 (1997).

[58] In Ref. [37], a q^{-2} scaling is found for discocyte fluctuation data in the range of wave vectors $0.002\ \mathrm{nm}^{-1} \lesssim q \lesssim 0.010\ \mathrm{nm}^{-1}$. When we analyze these data using our model, we conclude that the q^{-2} scaling may be fortuitous. In Ref. [25], the fitted surface tension term is only a minor contribution to the total effective bending rigidity, has approximately the magnitude of the q^{-2} perturbation term in Fig. 12, and never dominates the scaling behavior. However, the experimental data of Ref. [37] is consistent with the model in Ref. [25] as well as with the data measured in Ref. [36], and therefore supports the cytoskeleton confinement model.

[59] Fluctuation spectra are also discussed in Ref. [94]. The fluctuation amplitudes are found to scale like q^{-4} in the range of wavevectors $0.004\ \mathrm{nm}^{-1} \lesssim q \lesssim 0.019\ \mathrm{nm}^{-1}$. This scaling behavior indicates that the fluctuations at these wave vectors are governed only by a wave-vector-independent bending modulus. For some cells, the bending constant appears to be even smaller at small wave vectors compared with the values found at larger wave vectors. The data in Ref. [94] are not consistent with the data in Fig. 6 of Ref. [36]. Note that Ref. [94] mentions a different q range, $0.0007\ \mathrm{nm}^{-1} \leqslant \bar{\nu} \leqslant 0.003\ \mathrm{nm}^{-1}$ and claims that this range is for the wave *vectors*. However, the values are only reasonable if they give the wave *number*, $\bar{\nu} = 1/\lambda$, instead of the wave vector, $q = 2\pi/\lambda$. If the values would be wave vectors, the range would correspond to wavelengths between 2 μm and 9 μm. In the beginning of Ref. [94], it is stated that data for wavelengths between 0.25 μm and 3 μm have been measured. This latter range of wavelengths is reasonable with respect to the cell diameter of 8 μm.

[60] N. Gov and S. A. Safran, Phys. Rev. E **69**, 011101 (2004).

[61] C. Dubus and J. B. Fournier, Europhys. Lett. **75**, 181 (2006).

[62] F. Brochard-Wyart, N. Borghi, D. Cuvelier, and P. Nassoy, Proc. Natl. Acad. Sci. U.S.A. **103**, 7660 (2006).

[63] K. Zeman, H. Engelhard, and E. Sackmann, Eur. Biophys. J. **18**, 203 (1990).

[64] A. Roux, D. Cuvelier, P. Nassoy, J. Prost, P. Bassereau, and B.

Goud, EMBO J. **24**, 1537 (2005).
[65] J. Sleep, D. Wilson, R. Simmons, and W. Gratzer, Biophys. J. **77**, 3085 (1999).
[66] $\alpha_r = 5.4 \times 10^{-2} k_B T$ nm^{-1}, $\gamma = 1.5 \times 10^{-8} k_B T$ nm^{-4}.
[67] $\kappa_b = 9 k_B T$ and $\mu = 26 \times 10^{-2} k_B T$ nm^{-2} if the data are associated with fluctuations of the convex side of the stomatocyte.
[68] The renormalization α_r is determined self-consistently for a flat membrane, assuming that $\kappa_c \ll \alpha_r q^{-1}$ and $\kappa_s(r) \approx \alpha_r q^{-1}$. If there is a significant γq^{-4} contribution, this assumption might be not valid any more, since $\gamma q^{-4} \gg \alpha_r q^{-1}$ for small q. It thus might not be adequate to use both the q^{-1} term and the q^{-4} term in the same expression.
[69] H. J. Deuling and W. Helfrich, Biophys. J. **16**, 861 (1976).
[70] J. B. Manneville, P. Bassereau, D. Levy, and J. Prost, Phys. Rev. Lett. **82**, 4356 (1999).
[71] J. B. Manneville, P. Bassereau, S. Ramaswamy, and J. Prost, Phys. Rev. E **64**, 021908 (2001).
[72] P. Girard, J. Prost, and P. Bassereau, Phys. Rev. Lett. **94**, 088102 (2005).
[73] B. Rozycki, T. R. Weikl, and R. Lipowsky, Phys. Rev. E **73**, 061908 (2006).
[74] V. Bennett and D. M. Gilligan, Annu. Rev. Cell Biol. **9**, 27 (1993).
[75] M. P. Sheetz and J. Casaly, J. Biol. Chem. **255**, 9955 (1980).
[76] A. Zilker, H. Strey, and E. Sackmann, in *Structure and Conformation of Amphiphilic Membranes*, edited by R. Lipowsky, D. Richter, and K. Kremer, Vol. 66 of *Springer Proceedings in Physics* (Springer, Berlin, 1992).
[77] N. Gov, Phys. Rev. Lett. **93**, 268104 (2004).
[78] L. C. L. Lin, N. Gov, and F. L. H. Brown, J. Chem. Phys. **124**, 074903 (2006).
[79] We are aware of the fact that the effective temperature may be a function of the wave vector [87]. However, since the mechanism of the active fluctuations is not yet known, the use of a single, constant effective temperature is the simplest and most honest phenomenological approach.
[80] $T_{\mathrm{eff}}/T = 2.8$ and $\mu = 5.6 \times 10^{-2} k_B T$ nm^{-2} if the data are associated with fluctuations of the convex side of the stomatocyte.
[81] T. Auth and G. Gompper, Phys. Rev. E **72**, 031904 (2005).
[82] T. Bickel and C. M. Marques, Eur. Phys. J. E **9**, 349 (2002).
[83] M. W. Hetzer, T. C. Walther, and I. W. Mattaj, Annu. Rev. Cell Dev. Biol. **21**, 347 (2005).
[84] B. R. G. Johnson, R. J. Bushby, J. Colyer, and S. D. Evans, Biophys. J. **90**, L21 (2006).
[85] L. Limozin, M. Barmann, and E. Sackmann, Eur. Phys. J. E **10**, 319 (2003).
[86] J. Li, G. Lykotrafitis, M. Dao, and S. Suresh, Proc. Natl. Acad. Sci. U.S.A. **104**, 4937 (2007).
[87] N. S. Gov, Phys. Rev. E **75**, 011921 (2007).
[88] The upper integral boundary is taken to be infinity, which is valid if the fluctuation wave vectors of interest are much smaller than the cutoff wave vector that corresponds to the molecular size a, $q_c = 2\pi/a$. Especially for polymerized membranes when the molecular size is given by the mesh size of the network, the validity of this condition should be checked.
[89] It is reasonable to assume that there might be patches of missing or detached anchor proteins in red blood cells [74] (which correspond to a vanishing confining pressure in our model). Thus, locally, both membranes of the coupled membrane system have a considerably larger spacing in such regions of vanishing pressure. From Fig. 9, the gain in free energy by increasing the intermembrane distance d for a membrane patch of given size can be estimated. If the homogeneous pressure that keeps the membranes together vanishes for membrane areas of few hundred nm size, the free energy gained by a larger spacing is of the order of and larger than thermal energies (the chemical energy coupling the anchor points can be larger than $k_B T$ and is released): e.g., for $d = 30$ nm, $\mu = 0.01 k_B T$ nm^{-2}, and for a patch size of 10^4 nm^2, an increase of d by only 20 nm leads to a free energy gain of few $k_B T$.
[90] This choice has no influence on the results of the fits. Any other value for the normalization is also fine.
[91] This estimate is based on a constant bending rigidity of the network, $\kappa_c = 0.1 k_B T$ [25,51], and a shear modulus between $\mu = 2.4 \times 10^{-4} k_B T$ nm^{-1} and $\mu = 4.8 \times 10^{-2} k_B T$ nm^{-1} [32–35,65].
[92] Unless $\kappa_b \approx 1 k_B T$ (which is unreasonably small), also a higher value of κ_b does not allow to fit more data points.
[93] An alternative explanation, proteins or bipolar lipids embedded in the membrane, is suggested in Refs. [76,94].
[94] A. Zilker, M. Ziegler, and E. Sackmann, Phys. Rev. A **46**, 7998 (1992).